

A symbolic framework for flexible multibody systems applied to horizontal-axis wind turbines

Emmanuel Branlard¹ and Jens Geisler²

¹National Renewable Energy Laboratory, Golden, CO 80401, USA

²Hochschule Flensburg, University of Applied Sciences, 24943 Flensburg, Germany

Correspondence: E. Branlard (emmanuel.branlard@nrel.gov)

1 **Abstract.** The article presents a symbolic framework that is used to obtain the linear and nonlinear equations of motion
2 of a multibody system including rigid and flexible bodies. Our approach is based on Kane's method and a nonlinear shape
3 function representation for flexible bodies. The method yields compact symbolic equations of motion with implicit account
4 of the constraints. The general and automatic framework facilitates the creation and manipulation of models with various
5 levels of fidelity. The symbolic treatment allows for analytical gradients and linearized equations of motion. The linear and
6 nonlinear equations can be exported to Python code or dedicated software. There are multiple applications, such as time domain
7 simulation, stability analyses, frequency domain analyses, advanced controller design, state observers, and digital twins. In this
8 article, we describe the method we used to systematically generate the equations of motion of multibody systems. We apply
9 the framework to generate illustrative land-based and offshore wind turbine models. We compare our results with OpenFAST
10 simulations and discuss the advantages and limitations of the method. The Python implementation is provided as an open-
11 source project.

12 1 Introduction

13 The next generation of wind turbine digital technologies requires versatile aero-servo-hydro-elastic models, with various levels
14 of fidelity, suitable for a wide range of applications. Such applications include time domain simulations, linearization (for con-
15 troller design and tuning, or frequency domain analyses), analytical gradients (for optimization procedures), and generation of
16 dedicated, high-performance or embedded code (for stand-alone simulations, state observers or digital twins). Current models
17 are implemented for a specific purpose and are usually based on an heuristic structure. Aeroelastic tools, such as Flex (Øye,
18 1983; Branlard, 2019) or ElastoDyn (Jonkman et al., 2021), rely on an assumed chain of connections between bodies, a given
19 set of degrees of freedom, and predefined orientations of shape functions.

20 Tools with linearization capabilities, such as HAWCStab2 (Sønderby and Hansen, 2014) or OpenFAST (Jonkman et al.,
21 2021) are dedicated to horizontal-axis wind turbines, and the evaluation of the gradients are limited to hard-coded analytical
22 expressions or numerical finite differences. Small implementation changes often require extensive redevelopment, and the
23 range of applications of the tools remains limited (Simani, 2015).

24 To address this issue, we propose a framework for the automatic derivation, processing, and parameterization of models
25 with granularity in the level of fidelity. Our approach is based on Kane’s method (Kane and Wang, 1965) and a nonlinear
26 shape function representation of flexible bodies (Shabana, 2013) described using a standard input data (SID) format (Wallrapp,
27 1994; Schwertassek and Wallrapp, 1999). The method yields compact symbolic equations of motion with implicit account
28 of the constraints. Similar approaches have been presented in the literature: Kurz and Eberhard (2009), Merz (2018), Lem-
29 mer (2018), and Branlard (2019). Our framework differs in the fact that all equations are processed at a symbolic level and
30 therefore the model can be used in its nonlinear or linearized form. We implemented an open-source version in Python us-
31 ing SymPy (SymPy, 2021), leveraging its mechanical toolbox. Alternative symbolic frameworks found in the literature are
32 usually limited to rigid bodies (Verlinden et al., 2005; Kurz and Eberhard, 2009; Gede et al., 2013; Docquier et al., 2013) or
33 are closed-source (Reckdahl and Mitiguy, 1996; Kurtz et al., 2010; MotionGenesis, 2016) and cannot be directly processed in
34 Python.

35 Kane’s method and the nonlinear shape function approach presented in this article do not represent the state of the art
36 of multibody dynamics with flexible bodies. The geometrically exact beam theory (Simo, 1985; Jelenić and Crisfield, 1999;
37 G eradin and Cardona, 2001; Bauchau, 2011) is more precise than the shape function approach. Similarly, multipurpose multi-
38 body software exists (Lange et al., 2007), such as ANSYS (ANSYS, 2022), SIMPACK (SIMPACK, 2022), or MBDyn (MB-
39 Dyn, 2022). These more advanced approaches target different applications than those envisioned in this study: they are suitable
40 for numerical simulations, but they cannot provide simple and computationally efficient nonlinear and linear models.

41 In section 2, we present the formalism used to derive the equations of motion. In section 3, we given an overview of how the
42 equations were implemented into a symbolic calculation framework, to easily manipulate the equations and generate dedicated
43 code. Example of applications relevant to wind energy are given in section 4. Discussions and conclusions follow.

44 **2 Method to obtain the equations of motion**

45 In this section, we present the formalism used to setup the equations of motion.

46 **2.1 System definition and kinematics**

47 We consider a system of n_b bodies, rigid or flexible, connected by a set of joints. For simplicity, we assume that no kinematic
48 loops are present in the system, and the masses of the bodies are constant. An inertial frame is defined to express the positions,
49 velocities, and accelerations of the bodies. We adopt a minimal set of generalized coordinates, \mathbf{q} , of dimension n_q , to describe
50 the kinematics of the bodies: joint coordinates describing the joints displacements, and Rayleigh-Ritz coordinates for the
51 amplitudes of the shape functions of the flexible bodies (see, e.g., Branlard (2019)). The choice of coordinates is left to the
52 user, but it is assumed to form a minimal set. We will provide illustrative examples in section 4.

53 At a given time, the positions, orientations, velocities, and accelerations of all the points of the structure are entirely deter-
54 mined by the knowledge of \mathbf{q} , $\dot{\mathbf{q}}$, and $\ddot{\mathbf{q}}$, where (\cdot) represents the time derivative. For a given body i , and a point P belonging

55 to the body, the position, velocity, and acceleration of the point are given by (see, e.g., Shabana (2013)):

$$56 \quad \mathbf{r}_P = \mathbf{r}_i + \mathbf{s}_P = \mathbf{r}_i + \mathbf{s}_{P_0} + \mathbf{u}_P \quad (1)$$

$$57 \quad \mathbf{v}_P = \mathbf{v}_i + \boldsymbol{\omega}_i \times \mathbf{s}_P + (\dot{\mathbf{u}}_P)_i \quad (2)$$

$$58 \quad \mathbf{a}_P = \mathbf{a}_i + \boldsymbol{\omega}_i \times (\boldsymbol{\omega}_i \times \mathbf{s}_P) + \dot{\boldsymbol{\omega}}_i \times \mathbf{s}_P + 2\boldsymbol{\omega}_i \times (\dot{\mathbf{u}}_P)_i + (\ddot{\mathbf{u}}_P)_i \quad (3)$$

59 where \mathbf{r}_i , \mathbf{v}_i , and \mathbf{a}_i are the position, velocity, and acceleration of the origin of the body, respectively; \mathbf{s}_{P_0} is the initial
60 (undeformed) position vector of point P with respect to the body origin; the subscript P is used for the deformed position
61 of the point and P_0 for the undeformed position; \mathbf{u}_P is the elastic displacement of the point (equal to 0 for rigid bodies);
62 $\boldsymbol{\omega}_i$ is the rotational velocity of the body with respect to the inertial frame; (\cdot) and $(\cdot)_i$ refer to time derivatives in the inertial
63 and body frame respectively. Throughout the article, we use bold symbols for vectors and matrices, and uppercase symbols
64 for most matrices. The elastic displacement is obtained as a superposition of elastic deformations (see subsection 2.4). We
65 define the transformation matrix \mathbf{R}_i that transforms coordinates from the body frame to the inertial frame, and by definition
66 $[\tilde{\boldsymbol{\omega}}_i] = \dot{\mathbf{R}}_i \mathbf{R}_i^T$, where $[\tilde{\cdot}]$ represents the skew symmetric matrix, and the exponent T denotes the matrix transpose. We assume
67 that vectors are represented as column vectors to conveniently introduce matrix-vector multiplications. We use the notation “ \cdot ”
68 to indicate the dot product between two vectors (irrespective of their column or row representation).

69 2.2 Introduction to Kane’s method

70 Kane’s method (Kane and Wang, 1965) is a powerful and systematic way to obtain the equations of motion of a system. The
71 procedure leads to n_q coupled equations of motion:

$$72 \quad \mathbf{f}_r + \mathbf{f}_r^* = 0, \quad r = 1 \dots n_q \quad (4)$$

73 where \mathbf{f}_r^* is associated with inertial loads and \mathbf{f}_r is associated with external loads, and these components are obtained for all
74 generalized coordinates. The components are obtained as a superposition of contributions from each body:

$$75 \quad \mathbf{f}_r = \sum_{i=1}^{n_b} \mathbf{f}_{ri}, \quad \mathbf{f}_r^* = \sum_{i=1}^{n_b} \mathbf{f}_{ri}^* \quad (5)$$

76 The terms \mathbf{f}_{ri} and \mathbf{f}_{ri}^* can be obtained for each body individually and assembled at the end to form the final system of equa-
77 tions. We will present in subsection 2.3 and subsection 2.4 how these terms are defined for rigid bodies and flexible bodies,
78 respectively.

79 2.3 Rigid bodies

80 We assume that body i is a rigid body and proceed to define the terms \mathbf{f}_{ri} and \mathbf{f}_{ri}^* . The inertial force, \mathbf{f}_i^* , and inertial torque,
81 $\boldsymbol{\tau}_i^*$, acting on the body are:

$$82 \quad \mathbf{f}_i^* = -m_i \mathbf{a}_{G,i}, \quad \boldsymbol{\tau}_i^* = -\mathbf{I}_{G,i} \cdot \dot{\boldsymbol{\omega}}_i - \boldsymbol{\omega}_i \times (\mathbf{I}_{G,i} \cdot \boldsymbol{\omega}_i) \quad (6)$$

83 where m_i is the mass of the body, $\mathbf{a}_{G,i}$ is the acceleration of its center of mass with respect to the inertial frame, and $\mathbf{I}_{G,i}$ is the
 84 inertial tensor of the body expressed at its center of mass. Equation 6 is a vectorial relationship; it may therefore be evaluated
 85 in any coordinate system. The component f_{ri}^* is defined as:

$$86 \quad \mathbf{f}_{ri}^* = \mathbf{J}_{v,ri} \cdot \mathbf{f}_i^* + \mathbf{J}_{\omega,ri} \cdot \boldsymbol{\tau}_i^* \quad (7)$$

87 with

$$88 \quad \mathbf{J}_{v,ri} = \frac{\partial \mathbf{v}_{G,i}}{\partial \dot{q}_r}, \quad \mathbf{J}_{\omega,ri} = \frac{\partial \boldsymbol{\omega}_i}{\partial \dot{q}_r} \quad (8)$$

89 where $\mathbf{v}_{G,i}$ is the velocity of the body mass center with respect to the inertial frame. The partial velocities, or Jacobians, \mathbf{J}_v
 90 and \mathbf{J}_ω , are key variables of the Kane's method. They project the physical coordinates into the generalized coordinates (\mathbf{q}),
 91 inherently accounting for the kinematic constraints between bodies. In numerical implementations, the Jacobians are typically
 92 stored in matricial forms, referred to as "velocity transformation matrices." The terms \mathbf{f}_{ri}^* can equivalently be obtained using the
 93 partial velocity of any body point (e.g., the origin) by carefully transferring the inertial loads to the chosen point. The external
 94 forces and torques acting on the body are combined into an equivalent force and torque acting at the center of mass, written as
 95 \mathbf{f}_i and $\boldsymbol{\tau}_i$. The component \mathbf{f}_{ri} is then given by:

$$96 \quad \mathbf{f}_{ri} = \mathbf{J}_{v,ri} \cdot \mathbf{f}_i + \mathbf{J}_{\omega,ri} \cdot \boldsymbol{\tau}_i \quad (9)$$

97 Equivalently, the contributions from each individual force, $\mathbf{f}_{i,j}$, acting on a point P_j of the body i , and each torque, $\boldsymbol{\tau}_{i,k}$, can
 98 be summed using the appropriate partial velocity to obtain \mathbf{f}_{ri} :

$$99 \quad \mathbf{f}_{ri} = \sum_j \frac{\partial \mathbf{v}_{P_j}}{\partial \dot{q}_r} \cdot \mathbf{f}_{i,j} + \sum_k \mathbf{J}_{\omega,ri} \cdot \boldsymbol{\tau}_{i,k} \quad (10)$$

100 where \mathbf{v}_{P_j} is the velocity of the point j with respect to the inertial frame. Equation 7 and Equation 9 are inserted into Equation 5
 101 to obtain the final equations of motion.

102 2.4 Flexible bodies

103 We assume that body i is a flexible body and proceed to define the terms \mathbf{f}_{ri} and \mathbf{f}_{ri}^* . The dynamics of a flexible body are
 104 described in standards textbooks such as Shabana (2013) or Schwertassek and Wallrapp (1999). Unlike rigid bodies, the equa-
 105 tions for flexible bodies are typically expressed with respect to a reference point different from the center of mass. We will call
 106 this point the origin and write it O_i . The elastic displacement field of the body is written as \mathbf{u} . It defines the displacement of any
 107 point of the body with respect to its undeformed position. Using the zeroth-order¹ Rayleigh-Ritz approximation, the displace-
 108 ment field at a given point, P , is given by the sum of shape function contributions: $\mathbf{u}(P) = \sum_{j=1}^{n_{e,i}} \boldsymbol{\Phi}_{ij}(P) \mathbf{q}_{e,ij}(t)$, where $\boldsymbol{\Phi}_{ij}$
 109 are the shape functions (displacement fields) of body i , and $\mathbf{q}_{e,ij}$ is the subset of \mathbf{q} consisting of the elastic coordinates of body
 110 i , of size $n_{e,i}$. The principles of the shape function approach applied to beams are given in Appendix B. The shape functions

¹We address the first-order approximation in Appendix D4.

111 are more easily represented in the body coordinate system. Vectors and matrices that are explicitly written in the body frame
 112 will be written with primes. The equations of motion of the flexible bodies are (Wallrapp, 1994):

$$113 \begin{bmatrix} M'_{xx} & M'_{x\theta} & M'_{xe} \\ & M'_{\theta\theta} & M'_{\theta e} \\ \text{sym.} & & M'_{ee} \end{bmatrix}_i \begin{bmatrix} \mathbf{a}'_i \\ \dot{\boldsymbol{\omega}}'_i \\ \ddot{\mathbf{q}}_{e,i} \end{bmatrix} + \begin{bmatrix} \mathbf{k}'_{\omega,x} \\ \mathbf{k}'_{\omega,\theta} \\ \mathbf{k}'_{\omega,e} \end{bmatrix}_i + \begin{bmatrix} 0 \\ 0 \\ \mathbf{k}_e \end{bmatrix}_i = \begin{bmatrix} \mathbf{f}'_x \\ \mathbf{f}'_\theta \\ \mathbf{f}'_e \end{bmatrix}_i \quad (11)$$

114 where the x , θ , and e , subscripts respectively indicate the translation, rotation, and elastic components; \mathbf{M} is the mass matrix
 115 of dimension $6+n_{e,i}$ made of the block matrices M_{xx}, \dots, M_{ee} ; \mathbf{a}_i and $\dot{\boldsymbol{\omega}}_i$ are the linear and angular acceleration of the body
 116 (origin) with respect to the inertial frame; \mathbf{k}_ω are the centrifugal, gyration, and Coriolis loads, also called quadratic velocity
 117 loads; \mathbf{k}_e are the elastic strain loads, which may contain geometric stiffening effects; \mathbf{f} are the external forces, torques, and
 118 elastic generalized forces. The different components of \mathbf{M} , \mathbf{k}_ω , \mathbf{k}_e , and \mathbf{f} are given in Appendix A. These terms depend on \mathbf{q} ,
 119 $\dot{\mathbf{q}}$, and Φ_i . The inertial force, torque, and elastic loads are:

$$120 \mathbf{f}_i^* = -\mathbf{R}_i [M'_{xx}\mathbf{a}'_i + M'_{x\theta}\dot{\boldsymbol{\omega}}'_i + M_{xe}\ddot{\mathbf{q}}_{e,i} + \mathbf{k}'_{\omega,x}] \quad (12)$$

$$121 \boldsymbol{\tau}_i^* = -\mathbf{R}_i [M'_{\theta x}\mathbf{a}'_i + M'_{\theta\theta}\dot{\boldsymbol{\omega}}'_i + M_{\theta e}\ddot{\mathbf{q}}_{e,i} + \mathbf{k}'_{\omega,\theta}] \quad (13)$$

$$122 \mathbf{h}_i^* = - [M'_{ex}\mathbf{a}'_i + M'_{e\theta}\dot{\boldsymbol{\omega}}'_i + M_{ee}\ddot{\mathbf{q}}_{e,i} + \mathbf{k}'_{\omega,e}] \quad (14)$$

123 The external and elastic loads are:

$$124 \mathbf{f}_i = \mathbf{R}_i \mathbf{f}'_x \quad (15)$$

$$125 \boldsymbol{\tau}_i = \mathbf{R}_i \mathbf{f}'_\theta \quad (16)$$

$$126 \mathbf{h}_i = \mathbf{f}_e - \mathbf{k}_e \quad (17)$$

127 The components of \mathbf{f}_{ri}^* and \mathbf{f}_{ri} , for $r = 1 \dots n_q$, are then defined as:

$$128 \mathbf{f}_{ri}^* = \mathbf{J}_{v,ri} \cdot \mathbf{f}_i^* + \mathbf{J}_{\omega,ri} \cdot \boldsymbol{\tau}_i^* + \mathbf{J}_{e,ri} \cdot \mathbf{h}_i^* \quad (18)$$

$$129 \mathbf{f}_{ri} = \mathbf{J}_{v,ri} \cdot \mathbf{f}_i + \mathbf{J}_{\omega,ri} \cdot \boldsymbol{\tau}_i + \mathbf{J}_{e,ri} \cdot \mathbf{h}_i \quad (19)$$

130 with

$$131 \mathbf{J}_{v,ri} = \frac{\partial \mathbf{v}_{O,i}}{\partial \dot{q}_r}, \quad \mathbf{J}_{\omega,ri} = \frac{\partial \boldsymbol{\omega}_i}{\partial \dot{q}_r}, \quad \mathbf{J}_{e,ri} = \frac{\partial \mathbf{q}_{e,i}}{\partial q_r} \quad (20)$$

132 where $\mathbf{v}_{O,i}$ is the velocity of the body with respect to the inertial frame. The term $\mathbf{J}_{e,ri}$ consists of 0 and 1 because $\mathbf{q}_{e,i}$ is a
 133 subset of \mathbf{q} . Equation 18 and Equation 19, once evaluated for body i , are inserted into Equation 5 to obtain the final equations
 134 of motion.

135 2.5 Nonlinear and linear equations of motion

136 The n_q equations of motion given in Equation 4 are gathered into a vertical vector \mathbf{e} . They are recast into the form:

$$137 \mathbf{e}(\mathbf{q}, \dot{\mathbf{q}}, \ddot{\mathbf{q}}, \mathbf{u}, t) = \mathbf{f} + \mathbf{f}^* = \mathbf{F}(\mathbf{q}, \dot{\mathbf{q}}, \mathbf{u}, t) - \mathbf{M}(\mathbf{q})\ddot{\mathbf{q}} = \mathbf{0} \quad (21)$$

138 or

$$139 \quad M(\mathbf{q})\ddot{\mathbf{q}} = \mathbf{F}(\mathbf{q}, \dot{\mathbf{q}}, \mathbf{u}, t) \quad (22)$$

140 where $M = -\frac{\partial \mathbf{e}}{\partial \ddot{\mathbf{q}}}$ is the system mass matrix and \mathbf{F} is the forcing term vector—that is, the remainder terms of the equation
141 ($\mathbf{F} = \mathbf{e} + M\ddot{\mathbf{q}}$). The vector \mathbf{u} is introduced to represent the time-dependent inputs that are involved in the determination of the
142 external loads. Both sides of the equations are also dependent on some parameters, but this dependency is omitted to shorten
143 notations. The stiffness and damping matrices may be obtained by computing the Jacobian of the equations of motion with
144 respect to \mathbf{q} and $\dot{\mathbf{q}}$, respectively. The nonlinear equation given in Equation 22 is easily integrated numerically, for instance by
145 recasting the system into a first-order system, or by using a dedicated second-order system time integrator.

146 In various applications, a linear time invariant approximation of the system is desired. Such approximation is obtained at an
147 operating point, noted with the subscript 0, which is a solution of the nonlinear equations of motion, namely:

$$148 \quad \mathbf{e}(\mathbf{q}_0, \dot{\mathbf{q}}_0, \ddot{\mathbf{q}}_0, \mathbf{u}_0, t) = \mathbf{0} \quad (23)$$

149 The linearized equations about this operating point are obtained using a Taylor series expansion:

$$150 \quad M_0(\mathbf{q}_0)\delta\ddot{\mathbf{q}} + C_0(\mathbf{q}_0, \dot{\mathbf{q}}_0, \mathbf{u}_0)\delta\dot{\mathbf{q}} + K_0(\mathbf{q}_0, \dot{\mathbf{q}}_0, \ddot{\mathbf{q}}_0, \mathbf{u}_0)\delta\mathbf{q} = Q_0(\mathbf{q}_0, \dot{\mathbf{q}}_0, \mathbf{u}_0)\delta\mathbf{u} \quad (24)$$

151 with

$$152 \quad M_0 = -\left. \frac{\partial \mathbf{e}}{\partial \ddot{\mathbf{q}}} \right|_0, C_0 = -\left. \frac{\partial \mathbf{e}}{\partial \dot{\mathbf{q}}} \right|_0, K_0 = -\left. \frac{\partial \mathbf{e}}{\partial \mathbf{q}} \right|_0, Q_0 = \left. \frac{\partial \mathbf{e}}{\partial \mathbf{u}} \right|_0 \quad (25)$$

153 where M_0 , C_0 , and K_0 are the linear mass, damping, and stiffness matrices, respectively; $Q_0\delta\mathbf{u}$ is the linear forcing vector
154 (Q_0 is the input matrix); δ indicates a small perturbation of the quantities; and $|_0$ indicates that the expressions are evaluated at
155 the operating point. In practical applications, linearization is done at an operating point where the acceleration is zero ($\ddot{\mathbf{q}}_0 = 0$)
156 and most velocities are also zero. Examples of applications of the linear equations of motion are controller design, frequency
157 domain analyses, and stability analyses. The symbolic system matrices also allow for the easy formulation of linear parameter-
158 varying models used in many advanced control applications.

159 3 Implementation into a symbolic framework

160 In this section, we discuss a Python open-source symbolic calculation framework that implements the equations given in
161 section 2. A Maxima implementation from the same authors is also available Geisler (2021).

162 The Python library YAMS (Yet Another Multibody Solver) started as a numerical tool published in previous work (Bran-
163 lard, 2019). The library is now supplemented with a symbolic module so that both numerical and symbolic calculations can
164 be achieved. The new implementation uses the Python symbolic calculation package SymPy (SymPy, 2021). We leveraged the
165 features present in the subpackage “mechanics,” which contains all the tools necessary to compute kinematics: the definition
166 of frames and points and the determination of positions, velocities, and accelerations. The subpackage also contains an imple-
167 mentation of Kane’s equations for rigid bodies (i.e., subsection 2.3). We were also inspired by the package PyDy (Gede et al.,

168 2013), which is a convenient tool to export the equations of motion to executable code and directly visualize the bodies in 3D.
 169 The core of our work consisted of implementing a class to define flexible bodies (`FlexibleBody`) and the corresponding
 170 Kane’s method for this class (subsection 2.4).

171 For the `FlexibleBody` class, we followed the formalism of Wallrapp (1994) and implemented Taylor expansions for all
 172 the terms defined in Appendix A, allowing the symbolic computation with Taylor expansions to any order. In practice, a zeroth-
 173 or first-order expansion is used. The use of Taylor expansions is presented in Appendix D3. The different Taylor coefficients
 174 may be kept as symbolic terms, or replaced early on by numerical values provided by a SID, for instance.

175 We structured the code into three layers: 1) The low-level layer integrates seamlessly with SymPy and PyDy by using the
 176 `FlexibleBody` class we provide. It is the layer that offers the highest level of granularity and control for the user, since
 177 arbitrary systems with various kinematic constraints can be implemented, at the cost of requiring more expertise. 2) The
 178 second-level automates the calculation of the kinematics by introducing simple connections between rigid and flexible bodies.
 179 The connections may be rigid, with constant offsets and rotations, or dynamic. A connection from a flexible body to another
 180 body is assumed to occur at one extremity of the flexible body. Some knowledge of SymPy mechanics is still required to use
 181 this layer. 3) The third level consists of template models such as generic land-based or offshore wind turbine models. Degrees
 182 of freedom are easily turned on and off for these conceptual models depending on the level of fidelity asked by the user, and
 183 generic external forces can be implemented or declared as external inputs.

The overall workflow for typical usage of the symbolic framework is illustrated in Figure 1. The symbolic framework takes

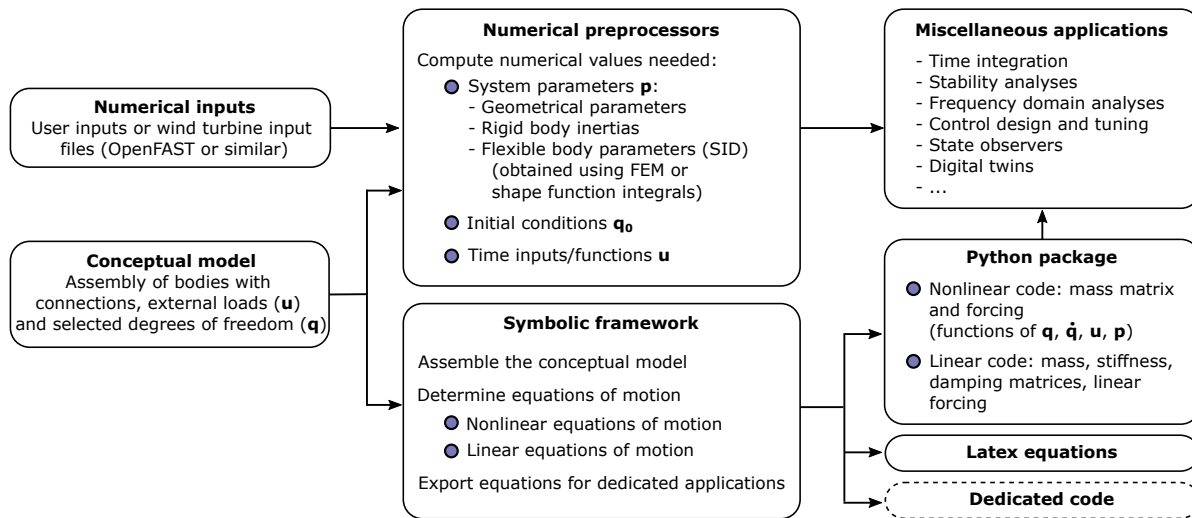


Figure 1. Typical workflow for the usage of the symbolic framework, going from numerical inputs and a conceptual model to numerical packages that can be used for various applications.

184
 185 as input a conceptual model of the structure, which is assembled using one of the three layers previously described. The
 186 nonlinear and linear equations of motion can be exported to LaTeX and Python-ready scripts for various applications (see
 187 subsection 5.1). Using the third layer, as little as three lines of code are required by the user to perform the full step from

188 derivation of the equations, optional linearization, and exportation. To obtain numerical results from the exported Python code,
189 the user needs to provide the arrays with the degrees of freedom values \mathbf{q} and $\dot{\mathbf{q}}$, their initial conditions, a dictionary with
190 inputs (\mathbf{u}) that are functions of time, and a dictionary of parameters (\mathbf{p}) containing all the numerical constants such as mass,
191 acceleration of gravity, and geometric parameters. We implemented various preprocessing tools in YAMS to facilitate the
192 calculation of numerical parameters, typically from a set of OpenFAST input files or by using structural parameters defined
193 by the users. YAMS contains tools to compute the flexible bodies parameters (mass matrix, stiffness matrix, shape integrals)
194 using integrals over the shape functions or using a finite-element beam formulation. YAMS also contains tools to compute the
195 rigid body inertia of different components of a wind turbine or the full system. Postprocessing tools are also included to readily
196 time-integrate the generated model using numerical values (including initial values).

197 The source code of YAMS is available on GitHub as a subpackage of the Wind Energy LIBrary, WELIB (Branlard, 2021).
198 The repository contains tests and working examples, including the ones presented in section 4.

199 4 Wind energy applications

200 4.1 Approach

201 In this section, we present different wind energy applications of the symbolic framework. We focus on models with at least
202 one flexible body because the rigid body formulation of SymPy has been well verified (Gede et al., 2013). For each example,
203 the equations of motion are given and their results are compared with OpenFAST (Jonkman et al., 2021) simulations. This
204 is readily achieved because our framework can export the equations of motion to Python functions, load input files from an
205 OpenFAST model, and integrate the generated equations using the same conditions as defined in the OpenFAST input files.
206 In this article, we do not focus on the modeling of the external loads, but we include them in the equations of motion. It is
207 the responsibility of the user to define these functions, for instance through aero- or hydro-force models. For the verification
208 results presented in this section, we only include the gravitational and inertial loading. In all examples, the National Renewable
209 Energy Laboratory (NREL) 5-MW reference wind turbine (Jonkman et al., 2009) is used. The examples below are provided
210 on the GitHub repository where the YAMS package is provided (Branlard, 2021).

211 4.2 Notations

212 We adopt a system of notations where the first letter of a body is used to identify the parameters of that body. As an example,
213 the tower is represented with the letter T, and the following body parameters are defined: T , origin; M_T , mass; L_T , length;
214 $(J_{x,T}, J_{y,T}, J_{z,T})$, diagonal coefficients of the inertia tensor about the center of gravity and in body coordinates; \mathbf{r}_{TG} , vector
215 from body origin to body center of mass, of coordinates (x_{TG}, y_{TG}, z_{TG}) in body coordinates. We also define θ_t , the nacelle
216 tilt angle about the y axis; g , the acceleration of gravity along $-z$; and O , the origin of the global coordinate system.

217 4.3 Rotating blade with centrifugal stiffening

218 We begin with the study of a flexible blade of length $L_B = R$, rotating at the constant rotational speed Ω . We use this test
 219 case to familiarize the reader with the key concepts of the shape function approach given in Appendix B. A sketch of the
 220 system is given in Figure 2. We start by modeling the blade using a single shape function, assumed to be directed along the
 x -axis (“flapwise”): $\Phi_1 = \Phi e_x$, where e_x is the unit vector in the x direction. The undeflected blade is directed along the radial

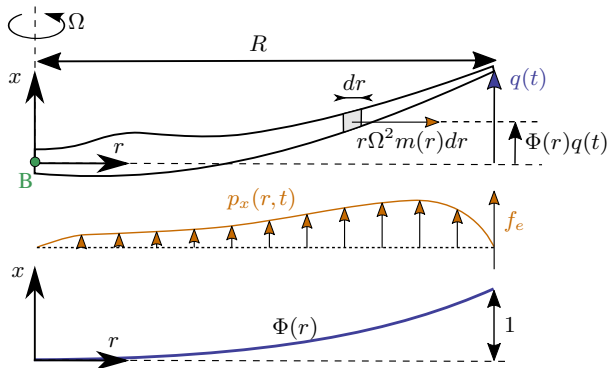


Figure 2. Sketch of a rotating blade with the restoring centrifugal force. Points are indicated in green, degrees of freedom in blue, and loads in orange.

221 coordinate r and rotates around the x -axis. We assume that the shape function is known, noted $\Phi(r)$. It can be computed as the
 222 first flapwise mode of the blade using tools provided in YAMS. The expression $\Phi(r) = r^3$ is a simple approximation that can
 223 be used for hand calculations. The aerodynamic force per length in the flapwise direction is noted $p_x(r)$. The generalized mass
 224 and stiffness are computed based on the mass per length (m) and flapwise bending stiffness (EI_y) of the blade, according to
 225 Equation B1:

$$227 \quad M_e = \int_0^R m(r) \Phi^2(r) dr \quad (26)$$

$$228 \quad K_e = \int_0^R EI_y(r) \left[\frac{d^2 \Phi}{dr^2}(r) \right]^2 dr \quad (27)$$

229 The generalized force is obtained from Equation B3:

$$230 \quad f_e = \int_0^R p_x(r,t) \Phi(r) dr \quad (28)$$

231 The important consideration for this model is the axial load, N . The main axial load at a radial station r comes from the
 232 centrifugal force acting on all the points outboard of the current station:

$$233 \quad N(r) = \int_r^R m(r') \Omega^2 r' dr' \quad (29)$$

234 The geometric stiffness contribution of the axial load is obtained from Equation B5 as:

$$235 \quad K_g(\Omega) = \int_0^R N(r) \left[\frac{d\Phi}{dr} \right]^2 dr = \Omega^2 \int_0^R \int_r^R m(r') r' dr' \left[\frac{d\Phi}{dr} \right]^2 dr \quad (30)$$

236 The geometric stiffness, K_g , is positive and increases with the square of the rotational speed. This restoring effect is referred
 237 to as “centrifugal stiffening.” The natural frequency of the blade will increase with the rotational speed as follows:

$$238 \quad \omega_0(\Omega) = \sqrt{\frac{(K_e + K_g(\Omega))}{M_e}} = \sqrt{\omega_0^2(0) + \frac{K_g(\Omega)}{M_e}} = \sqrt{\omega_0^2(0) + k_\Omega \Omega^2} \quad (31)$$

239 where k_Ω is referred to as the “rise factor” or “Southwell coefficient,” and in our approximation, it is found to be constant:
 240 $k_\Omega = K_g(\Omega)/M_e/\Omega^2$. The coefficient provides the variation of the blade frequency with rotational speed, which is something
 241 that is observed on a Campbell diagram when performing stability analyses. In general, the mode shapes of the blade will also
 242 change as a function of the rotational speed, and different shape functions should preferably be used for simulations at different
 243 rotational speeds. The effect is fairly limited, and most OpenFAST practitioners only use one shape function corresponding to
 244 the value at rated rotational speed. Similarly, the Southwell coefficient is a function of the rotational speed, but the variation is
 245 negligible as long as the rotational speed is small compared to the natural frequency (e.g., $(\Omega/\omega)^2 \lesssim 5$; see Bielawa (2006)),
 246 which is the case for wind energy applications.

247 The treatment for a shape function in the edgewise direction is similar, using $\Phi_2 = \Phi_2 e_\theta$, where e_θ is the unit vector
 248 in the edgewise direction. In this case, the centrifugal force also has a component in the tangential direction, $p_{\theta, \text{centri}}(r) =$
 249 $-\Omega^2 u_\theta(r) dm(r)$, with $u_\theta = \Phi_2 q$. This leads to a generalized force equal to $\int_0^L p_{\theta, \text{centri}} \Phi_2 dr = -\Omega^2 M_e q$, or, equivalently, to a
 250 stiffness term: $K_\omega = -\Omega^2 M_e$. It can be verified that this generalized force corresponds to the contribution $O_{e,11} \omega_x^2$, from $\mathbf{k}_{\omega, e}$,
 251 given in Equation A10. For an edgewise mode, the frequency therefore evolves as:

$$252 \quad \omega_0(\Omega) = \sqrt{\frac{(K_e + K_g(\Omega) + K_\omega(\Omega))}{M_e}} = \sqrt{\omega_0^2(0) + (k_\Omega - 1)\Omega^2} \quad (32)$$

253 with $k_\Omega = K_g(\Omega)/M_e/\Omega^2$ and with K_g computed using Equation 30.

254 We apply the method to the NREL 5-MW wind turbine using the blade properties and shape functions provided in the Elas-
 255 toDyn input file. We order the degrees of freedom as 1st flap, 1st edge, and 2nd flap, assuming no coupling between the shape
 256 functions, so that each can be treated individually using the results from this section. The diagonal coefficients of the mass ma-
 257 trix are $\text{diag}(\mathbf{M}_e) = [9.5e3, 1.5e4, 5.7e3]$, and for the stiffness matrix they are $\text{diag}(\mathbf{K}_e) = [1.7e4, 6.7e4, 8.7e4]$, computed
 258 according to Equations 26 and 27. The coefficients k_Ω of each degree of freedom are obtained as $\mathbf{k}_\Omega = [1.7, 1.4, 5.5]$. We

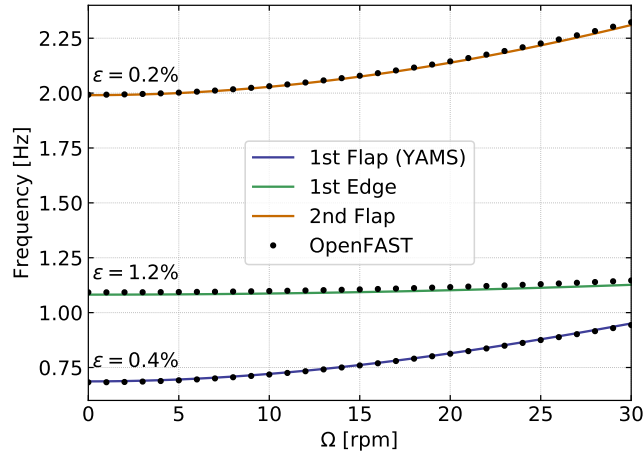


Figure 3. Variation of the natural frequencies of the NREL 5-MW turbine blade with rotational speed. Results from YAMS and OpenFAST, with mean relative error, ϵ , are reported on the figure.

259 compare the frequencies obtained with the present method against OpenFAST linearization results in Figure 3. The simulations
 260 were run in vacuum (no gravity, no aerodynamics) and with a cone angle of 0 deg. Strong agreement is found for the evolution
 261 of the different frequencies with the rotational speed. The stiffening is less pronounced for edgewise modes as a result of the
 262 softening introduced by K_ω .

263 This section focused on the analysis of individual shape functions. In the general case, multiple shape functions are present
 264 and couplings might exist between them (due to the structural twist or nonorthogonality of the shape functions, or if the shape
 265 functions have components in multiple directions such as $\Phi_1 = \Phi_{1x}e_x + \Phi_{1y}e_y$). In such a case, the general developments of
 266 Appendix A and Appendix B should be used.

267 4.4 Two degrees of freedom model of a land-based or fixed-bottom turbine

268 We consider a system of three bodies: tower (or support structure), nacelle, and rotor. The system represents a land-based
 269 wind turbine or a fixed-bottom offshore wind turbine. A sketch of the system is given in Figure 4. The nacelle and rotor
 270 blades are rigid bodies, whereas the tower is flexible and represented by one shape function² in the fore-aft direction, noted
 271 $\Phi_1 = \Phi_{1x}e_x$. For hand calculations and as a first approximation, the first mode shape of a massless beam with a top mass
 272 may be used: $\Phi_1(z) = 1 - \cos(z\pi/L/2)$. Increased accuracy is obtained when the shape function matches the actual first
 273 tower fore-aft bending mode, accounting for the effect of the rotor-nacelle mass and inertia. The degrees of freedom are
 274 $q = (q, \psi)$, where q is the generalized (elastic) coordinates in the fore-aft direction and ψ is the azimuthal position. The
 275 slope of the tower shape function at the tower top is a key coupling parameter of the model, noted ν_y . When the tower
 276 deflects 1 m in the x direction, the nacelle rotates by an angle ν_y . The method assumes that the tower-top point remains
 277 along the x -axis, neglecting the so-called nonlinear geometric effect. However, nonlinear geometric effects can be included

²The relevant equations of the shape function approach for a beam are given in Appendix B.

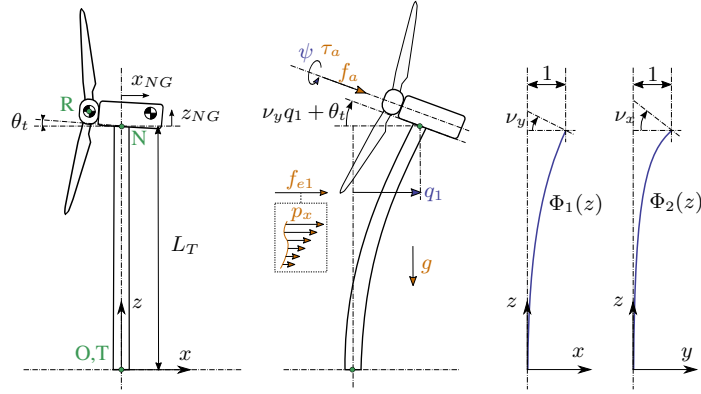


Figure 4. Model of a land-based or fixed-bottom wind turbine using one to three degrees of freedom (fore-aft and side-side flexibility of the support structure, and shaft rotation). Points are indicated in green, degrees of freedom in blue, and loads in orange.

278 using geometric stiffening corrections (see Appendix C or Branlard (2019)). The aerodynamic thrust and torque are noted
 279 f_a and τ_a , respectively, and act at the rotor center (point R). The low-speed shaft generator torque is written as τ_g . The
 280 distributed loads on the tower, p_x (from aerodynamics and hydrodynamics), are projected against the shape function to obtain
 281 the generalized forces $f_e = \int_0^{L_T} p_x(z, t) \Phi_1(z) dz$. The moments of inertia of the rotor in its coordinates are $(J_{x,R}, J_{\oplus,R}, J_{\ominus,R})$.
 282 We note that M_e, K_e , and D_e are the generalized mass, stiffness, and damping, respectively, associated with a given shape
 283 function $M_e = \int_0^{L_T} m(z) \Phi_1^2(z) dz$, $K_e = \int_0^{L_T} EI(z) \left[\frac{d^2 \Phi_1}{dz^2}(z) \right]^2 dz$, $D_e = 2\zeta M_e \omega_e$. where $m(z)$ and $EI(z)$ are the mass
 284 per length and bending stiffness of the tower, respectively, and ω_e and ζ are the frequency and damping ratio, respectively,
 285 associated with the shape function (assuming the shape function approximates a mode shape). The geometric softening of the
 286 tower due to the tower-top mass (K_{gt}) and its own weight (K_{gw}) is obtained using Equation B5, as $K_g = K_{gt} + K_{gw}$, with :

$$287 \quad K_{gt} = -g \int_0^{L_T} (M_R + M_N) \left[\frac{d\Phi_1}{dz}(z) \right]^2 dz \quad (33)$$

$$288 \quad K_{gw} = -g \int_0^{L_T} \left[\frac{d\Phi_1}{dz}(z) \right]^2 \left[\int_z^{L_T} m(z') dz' \right] dz \quad (34)$$

289 The shape function frequency is obtained as:

$$290 \quad \omega_e = \sqrt{(K_e + K_g)/M_e} \quad (35)$$

291 The application of the symbolic framework leads to the following equations of motion (rearranged for interpretability):

$$292 \quad \begin{bmatrix} M_q & 0 \\ 0 & J_{x,R} \end{bmatrix} \begin{bmatrix} \ddot{q} \\ \ddot{\psi} \end{bmatrix} = \begin{bmatrix} f_q \\ \tau_a - \tau_g \end{bmatrix} \quad (36)$$

293 where:

$$294 \quad M_q = M_e + M_N + M_R \quad (37)$$

$$295 \quad + (J_{yN} + J_{\oplus,R} + M_N(x_{NG}^2 + z_{NG}^2) + M_R(x_{NR}^2 + z_{NR}^2))\nu_y^2 \quad (38)$$

$$296 \quad + 2[(M_N z_{NG} + M_R z_{NR}) \cos(\nu_y q) - (M_N x_{NG} + M_R x_{NR}) \sin(\nu_y q)] \nu_y \quad (39)$$

297 and

$$298 \quad f_q = f_e - (K_e + K_g)q - D_e \dot{q} \quad (40)$$

$$299 \quad + g\nu_y [(M_N x_{NG} + M_R x_{NR}) \cos(\nu_y q) + (M_N z_{NG} + M_R z_{NR}) \sin(\nu_y q)] \quad (41)$$

$$300 \quad + \nu_y^2 \dot{q}^2 [(M_N x_{NG} + M_R x_{NR}) \cos(\nu_y q) + (M_N z_{NG} + M_R z_{NR}) \sin(\nu_y q)] \quad (42)$$

$$301 \quad + f_a \nu_y (x_{NR} \sin \theta_t + z_{NR} \cos \theta_t) \quad (43)$$

$$302 \quad + f_a \cos(\theta_t + \nu_y q) \quad (44)$$

303 Details on the derivations are given in Appendix E1. The mass matrix consists of three main contributions: Equation 37
 304 represents the elastic mass and the rotor nacelle assembly (RNA) mass, Equation 38 is the generalized rotational inertia of the
 305 RNA, and Equation 39 is the inertial coupling between the tower bending and the rotation of the nacelle. The forcing terms
 306 are identified as follows: Equation 40 consists of the elastic load resulting from the external forces on the tower, the elastic and
 307 geometric stiffness loads, and the damping load on the tower; Equation 41 is the gravitational load from the RNA, which will
 308 contribute to the stiffness of the system; Equation 42 is the centrifugal force of the RNA (“ $M\omega^2 r$ ” with $\omega = \nu_y \dot{q}$); Equation 43
 309 is the generalized torque from the aerodynamic thrust; and Equation 44 is the thrust contribution acting directly along the
 310 direction of the shape function degree of freedom (along x). The RNA center of mass plays an important part in the equations
 311 (see the terms $(M_N x_{NG} + M_R x_{NR})$ and $(M_N z_{NG} + M_R z_{NR})$).

312 The equations of motion given in Equation 36 can be used to perform time domain simulations of a wind turbine. It is noted
 313 that the two degrees of freedom are only coupled by the aerodynamic loads. The nonlinear model was used in previous work
 314 for time domain simulations and its linear version was used for state estimations (Branlard et al., 2020a, b). In this section,
 315 we apply the linearized form to compute the natural frequency of the turbine tower fore-aft mode. The linearized stiffness is
 316 obtained by taking the gradient of the forcing with respect to q , and using a small angle approximation for ν_y to the second
 317 order:

$$318 \quad K_{q,lin} = (K_e + K_g) - \nu_y^2 g (M_N z_{NG} + M_R z_{NR} - f_a q \cos \theta_t) + \nu_y f_a \sin \theta_t \quad (45)$$

319 For the NREL 5-MW reference turbine (Jonkman et al., 2009), the different numerical values are: $g = 9.807 \text{ m} \cdot \text{s}^{-2}$, $\theta_t = 5$
 320 deg, $x_{NR} = -5.0 \text{ m}$, $z_{NR} = 2.4 \text{ m}$, $L_T = 87.6 \text{ m}$, $z_{NG} = 1.75 \text{ m}$, $x_{NG} = 1.9 \text{ m}$, $M_R = 1.1e5 \text{ kg}$, $J_{x,R} = 3.86e7 \text{ kg m}^2$,
 321 $J_{\oplus,R} = 1.92e7 \text{ kg m}^2$, $M_N = 2.4e5 \text{ kg}$, $J_{y,N} = 1.01e6 \text{ kg m}^2$, $M_{RNA} = 3.5e5 \text{ kg}$. The first fore-aft shape function of the

322 NREL 5-MW turbine tower and its derivatives are:

$$323 \quad \Phi_1(z) = (a_2 \bar{z}^2 + a_3 \bar{z}^3 + a_4 \bar{z}^4 + a_5 \bar{z}^5 + a_6 \bar{z}^6) / (a_2 + a_3 + a_4 + a_5 + a_6)$$

$$324 \quad \frac{d\Phi_1}{dz}(z) = \frac{1}{L_T} (2a_2 \bar{z} + 3a_3 \bar{z}^2 + 4a_4 \bar{z}^3 + 5a_5 \bar{z}^4 + 6a_6 \bar{z}^5) / (a_2 + a_3 + a_4 + a_5 + a_6) \quad (46)$$

$$325 \quad \frac{d^2\Phi_1}{dz^2}(z) = \frac{1}{L_T^2} (2a_2 + 6a_3 \bar{z} + 12a_4 \bar{z}^2 + 20a_5 \bar{z}^3 + 30a_6 \bar{z}^4) / (a_2 + a_3 + a_4 + a_5 + a_6)$$

326 with $\bar{z} = z/L$, $a_2 = 0.7004$, $a_3 = 2.1963$, $a_4 = -5.6202$, $a_5 = 6.2275$, and $a_6 = -2.504$. The material properties and the shape function are illustrated in Figure 5. The scaling of the shape functions given in Equation 46 is important to obtain the correct

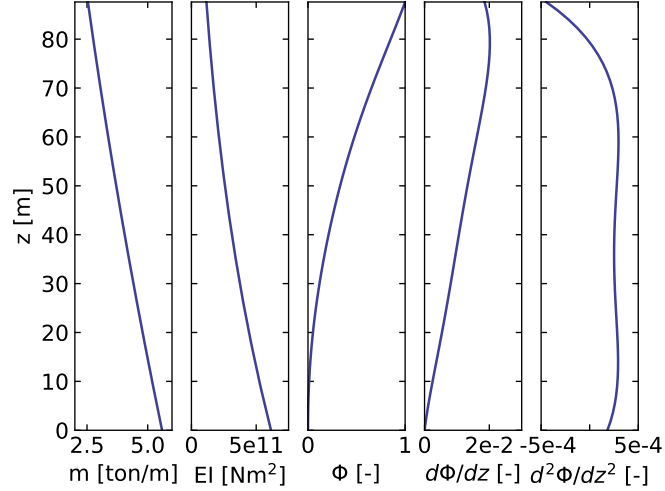


Figure 5. Properties of the NREL 5-MW turbine tower: mass per length (m), bending stiffness (ET), and shape function displacement (Φ), slope ($d\Phi/dz$) and curvature ($d^2\Phi/dz^2$).

327

328 numerical values for the flexible tower, namely: $\nu_y = 0.0185$, $M_e = 5.4e4$, $K_e = 1.91e6$, $K_g = -5.2e4 - 1.0e4 = -6.20e4$,

329 $\omega_e = \sqrt{(K_e + K_g)/M_e} = 5.85$ rad/s. These numerical values, with $q = 0$, lead to: $M_q = 4.375e5$ and $K_q = 1.849e9$. The

330 first fore-aft mode of the wind turbine has a natural frequency of $f = \sqrt{K_q/M_q} = 0.3272$ Hz. This value was compared with

331 results obtained using OpenFAST linearization. Both methods are in strong agreement, with differences only arising at the fifth

332 decimal place.

333 4.5 Three-degrees-of-freedom model of a land-based or fixed-bottom turbine

334 We consider the same system as the one presented in subsection 4.4, but the tower is now represented by one shape function in

335 both the fore-aft and side-side directions, $\Phi_1 = \Phi_1 e_x$ and $\Phi_2 = \Phi_2 e_y$. The degrees of freedom are $\mathbf{q} = (q_1, q_2, \psi)$, where q_1

336 and q_2 are the generalized (elastic) coordinates in the fore-aft and side-side directions, respectively, and ψ is the rotor azimuth.

337 A sketch of the system is given in Figure 4.

338 The slopes of the shape functions at the tower top are key coupling parameters of the model, noted ν_x and ν_y . The aerody-
 339 namic thrust and torque are noted f_a and τ_a , acting at point R . The distributed loads on the tower, p_x and p_y (from aerodynam-
 340 ics and hydrodynamics), are projected against the shape functions to obtain the generalized forces $f_{e1} = \int \Phi_1 p_x dz$ and $f_{e2} =$
 341 $\int \Phi_2 p_y dz$. The moments of inertia of the rotor in its coordinates are $(J_{x,R}, J_{\oplus,R}, J_{\oplus,R})$. We note that M_e , K_e , and D_e are
 342 the generalized mass, stiffness, and damping, respectively, associated with a given shape function (e.g., $M_{e11} = \int \Phi_1^2 m(z) dz$,
 343 where m is the mass per length of the tower). The application of the symbolic framework leads to the equations of motion
 344 given in Appendix E2. To simplify the equations and limit their length when printing them in this article, we have applied a
 345 first-order small-angle approximation for θ_t , and a second-order approximation for ν_x and ν_y . It is observed from Equation E14
 346 that a first-order approximation for ν_y would have removed the influence of the rotor and nacelle y -inertia on the generalized
 347 mass associated with the tower fore-aft bending.

348 We performed a time simulation of the model using both our symbolic framework YAMS and OpenFAST. The time integra-
 349 tion in YAMS currently relies on tools provided in the SciPy package, which implements several time integrators. A sufficient
 350 level of accuracy was obtained using a fourth-order Runge-Kutta method, which is the default method. Kane's method, which
 351 uses a minimal set of coordinates, tends to lead to stiff systems, and it is possible that implicit integrators may be needed for
 352 other systems. We compare the time series obtained using our generated functions with results from the equivalent OpenFAST
 353 simulation in Figure 6. In this simulation, the tower top is initially displaced by 1 m in the x and y directions, and the rotational
 speed is 5 rpm. We report the mean relative error, ϵ , and the coefficient of determination, R^2 , on the figure. We observe that

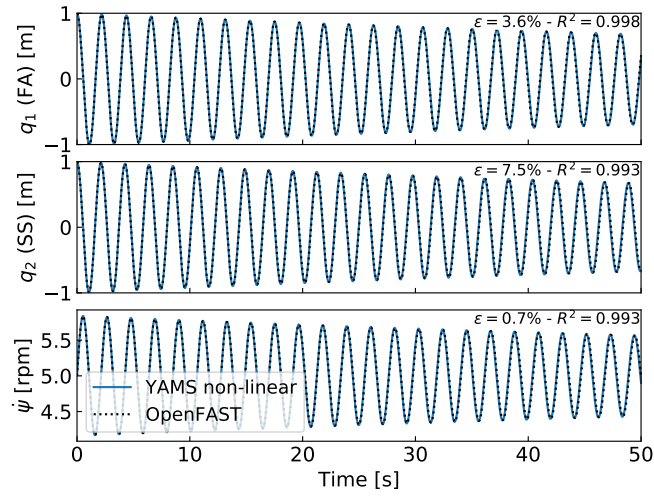


Figure 6. Free decay results for the land-based/fixed-bottom model using both the symbolic framework (YAMS) and OpenFAST. From top to bottom: tower fore-aft bending, tower side-side bending, and shaft rotational speed.

354
 355 our model is in strong agreement with the OpenFAST simulation. The differences in the second tower degree of freedom are
 356 attributed to 1) the handling of the small-angle approximation, which is different in OpenFAST (using the closest orthonormal
 357 matrix; Jonkman (2009)) and in our formulation (two successive rotations, linearized); 2) the nonlinear geometric corrections

358 that are implemented in OpenFAST, which we have omitted here by only selecting shape function expansion to the zeroth order
 359 (see subsection 5.2). The variation in azimuthal speed, resulting from the coupling between the gyroscopic loads and the tower
 360 bending, is captured well.

361 4.6 Three-degrees-of-freedom model of a floating wind turbine

362 In this example, we demonstrate the applicability of the method for a floating wind turbine. We model the turbine using three
 363 bodies: rigid floater, flexible tower, and rigid RNA (labeled ‘‘N’’). The degrees of freedom selected are: $q = (x, \phi, q_T)$, where x
 364 is the floater surge, ϕ is the floater pitch, and q_T is the coordinate associated with a selected fore-aft shape function. A sketch
 of the model is given in Figure 7. The notations are similar to the ones presented in subsection 4.5. Lumped hydrodynamic

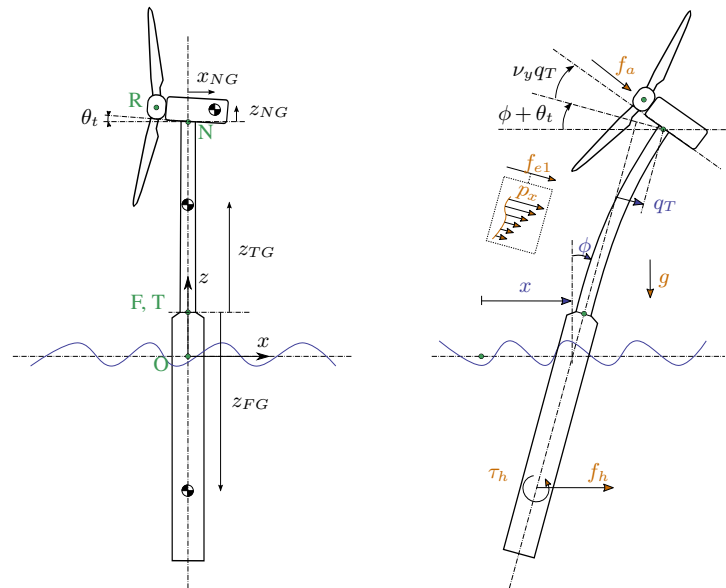


Figure 7. Model of a floating wind turbine using three degrees of freedom. Points are indicated in green, degrees of freedom in blue, and loads in orange.

365 loads at the floater center of mass are now added. The model can also be used for a combined tower and floater that is flexible,
 366 simply by setting the mass of the floater to zero and including the hydrodynamic loading into the loading p_x . The equations of
 367 motion are given in Appendix E3. The equations were simplified using a first-order small-angle approximation of θ_t and ϕ_y ,
 368 and a second-order approximation for ν_y .

370 We performed a numerical simulation of the model generated by YAMS and compared it with OpenFAST for a case with
 371 gravitational loads only, starting with $x = 0$ m, $\phi = 2$ deg, and $q_T = 1$ m. The results are presented in Figure 8. We observe
 372 again that the results from the two models correlate to a high degree.

373 We also compared the linearized version of both models. The symbolic framework can generate the linearized mass, stiffness,
 374 and damping matrices, as described in subsection 2.5. The matrices are then combined into a state matrix and compared with

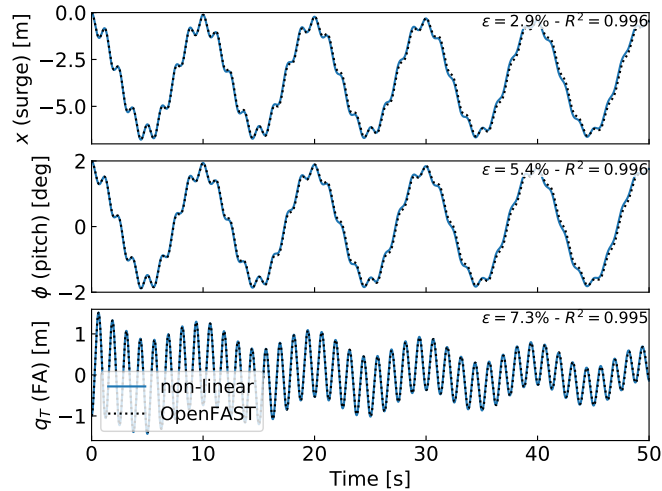


Figure 8. Free-decay results for the floating wind turbine model using YAMS and OpenFAST. From top to bottom: surge, pitch, and tower fore-aft bending.

375 the state matrices written by the OpenFAST linearization feature. The eigenvalue analysis of the YAMS state matrix returned
 376 a pitch and fore-aft frequencies of 0.099 Hz and 0.799 Hz, respectively, whereas OpenFAST returned 0.095 Hz and 0.795 Hz.
 377 The 4% error in the pitch frequency appears reasonable in view of the approximations used.

378 5 Discussions

379 5.1 Applications and advantages of the method

380 The implementation of the symbolic YAMS library was originally motivated by the need to obtain a simple linearized model
 381 of a floating wind turbine for frequency domain simulations. There are multiple potential applications of the framework:

- 382 – The generated equations can be used in time domain simulation tools. The equations can be readily exported to different
 383 programming languages (C, FORTRAN, or Python) providing computationally efficient tools, particularly because the
 384 method generates compact and minimal equations. This is in contrast to most other multibody codes, in which many
 385 terms are calculated as matrix equations and through successive function calls. Further, the symbolic framework allows
 386 us to generate optimized code, in which common terms and factors are computed once and stored in temporary variables
 387 for reuse in the different expressions. In our examples, time domain simulations were observed to be 2 orders of mag-
 388 nitude faster when using the automatically generated code in Python compared to OpenFAST simulations that rely on a
 389 compiled language. Using such a framework can be considered in the future to replace the existing ElastoDyn module
 390 of OpenFAST. It can also be applied to unusual configurations such as multirotor or vertical-axis turbine concepts. Ded-
 391 icated code can be generated for specific applications for increased performance. For instance, implicit integrators with

- 392 iterative Newton-Raphson-like solvers benefit from the possibility of generating exact and efficient Jacobians along with
393 the equations of motion.
- 394 – The generation of linearized models has a wide range of applications, such as linear time domain simulations, controller
395 design and tuning, frequency domain analyses, stability analyses, state observers, or digital twins. The symbolic approach
396 is severalfold faster than alternative approaches because it can be evaluated for all operating points at once, whereas other
397 methods (e.g., OpenFAST, HAWCStab2) require multiple linearization calls.
 - 398 – Analytical linearization with respect to parameters is directly obtained using our tool, which can be used for sensitivity
399 analyses, parameter studies, optimizations, integrated design approaches, and controls co-design (e.g., using methods
400 such as linear-matrix-inequality-based designs) (Pöschke et al., 2020). Nonanalytical approaches require numerous lin-
401 earizations and evaluations at various operating points (Jonkman et al., 2022).
 - 402 – In addition to the nonlinear or linear equations of motion in minimal coordinates, the equations for the constraint forces
403 or any auxiliary kinematic variable can also be generated efficiently by inserting unknown virtual displacements in the
404 equations (see Appendix D5 for an alternative approach). The position of all bodies in local or global coordinates can
405 be recovered from the minimal coordinates and, in combination with the flexible code generation, be used to output data
406 (e.g., for 3D animations of the turbine).
 - 407 – Analytical gradients of the equations can be computed and used in optimizations, nonlinear model predictive control,
408 or moving horizon estimation. External loads that cannot be expressed analytically can be defined as generic functions
409 of the structural degrees of freedom, inputs, and parameters. After the code generation, the user can link a numerical
410 implementation of the function and its numerical gradients to be able to use a mix of analytical and numerical gradients.
 - 411 – Another advantage of the presented method is the possibility to quickly generate models with different levels of de-
412 tail, ensuring consistency between the different levels of fidelity. This is in contrast to other more heuristic modeling
413 approaches in which parameters often have to be retuned for each added degree of freedom.
 - 414 – The method provides useful insights and can be used as an educational tool: simple models of a system with few degrees
415 of freedom can readily be obtained, studied, and compared to hand-based calculation.

416 **5.2 Advanced consideration**

417 Section 2 addressed the systematic derivation of the equations of motion for an assembly of rigid or flexible bodies. Some
418 advanced aspects of the method are discussed here:

- 419 – The different terms involved in the equations of motion of flexible bodies can be decomposed using shape integrals (see
420 Appendix D3). Our framework readily supports this optional decomposition: it is the responsibility of the user to provide
421 the terms and values of the expansion when numerical evaluation is to occur.

- 422 – The definition of geometric stiffening requires attention in the general case. It is accounted for by the term k_σ , presented
423 in Appendix A. We discuss geometric stiffening in more detail in Appendix C.
- 424 – The treatment of external loads was not addressed in detail in this article because the loads are application-specific (aero-
425 dynamics, hydrodynamics, etc.). The framework can accept external loads as arbitrary functions of multiple variables or
426 as analytical expressions. In the former case, the user will have to provide an implementation of the function during the
427 execution.
- 428 – Even though the equations of motion are void of constraint forces, the values of these forces can be recovered. They
429 can be expressed as functions of the external forces and the states of the system. It is not necessary to compute them by
430 iteratively solving constraint equations.
- 431 – The framework can easily include rheonomous constraints—for instance, for the pitch angle—without having to supply
432 a dedicated torque. Pitch speed and accelerations can be directly introduced into the mechanical system if they are
433 provided by a generic second-order pitch actuator model.

434 5.3 Limitations

435 In spite of the advantages listed in subsection 5.1, the symbolic procedure presented in this work has some potential limitations.
436 We are identifying two in this section. First, constraints and closed loops have currently not been added to the framework.
437 The SymPy mechanics package supports additional constraint equations within Kane’s method. We therefore hope that this
438 limitation can be lifted in the future. Second, large problems may challenge a symbolic calculation package: memory impact,
439 calculation time, simplification times, and size of expressions may become significant. Some of these issues may be alleviated
440 by introducing intermediate variables that are only substituted for in the numerical implementation or by using a recursive
441 formulation of the solution procedure (Branlard, 2019).

442 6 Conclusions

443 We presented a symbolic framework to obtain the linear and nonlinear equations of motion of a multibody system made of
444 rigid bodies, flexible bodies, and kinematic joints. Our approach is based on Kane’s method and a nonlinear shape function
445 representation of flexible bodies. We provided different wind energy examples and verified the results against OpenFAST
446 simulations. The framework can readily provide models suitable to a wide range of applications with competitive computational
447 times. The framework is open source, and the examples presented are available in the repository. Future work will focus on
448 applying the framework to dedicated research projects, with more complex systems, and potentially extend the framework to
449 account for closed-loop systems and arbitrary constraints.

450 *Author contributions.* Both authors exchanged over the last two years about the implementation of such a framework and its application to
 451 wind energy. EB wrote a Python implementation and JG wrote a Maxima implementation. EB wrote the main corpus of the article, with
 452 feedback and contributions from JG.

453 *Competing interests.* No competing interests are present.

454 *Code availability.* A Zenodo link will be created for <https://github.com/ebranlard/yams>. The examples given in this articles are found in the
 455 folder `welib/yams/papers` of the repository.

456 *Acknowledgements.* This work was authored in part by the National Renewable Energy Laboratory, operated by Alliance for Sustainable
 457 Energy, LLC, for the U.S. Department of Energy (DOE) under Contract No. DE-AC36-08GO28308. Funding provided by U.S. Department
 458 of Energy Office of Energy Efficiency and Renewable Energy Wind Energy Technologies Office. The views expressed in the article do
 459 not necessarily represent the views of the DOE or the U.S. Government. The U.S. Government retains and the publisher, by accepting the
 460 article for publication, acknowledges that the U.S. Government retains a nonexclusive, paid-up, irrevocable, worldwide license to publish or
 461 reproduce the published form of this work, or allow others to do so, for U.S. Government purposes.

462 *Financial support.* This work was funded under the Technology Commercialization Fund Project, supported by the DOE's Wind Energy
 463 Technologies Office.

464 **Appendix A: Equations for a flexible body and shape integrals**

465 In this section, we detail the equations of motion of a flexible body. The reader is referred to the following references for a complete treatment
 466 of the equations of motion: Shabana (2013), Schwertassek and Wallrapp (1999), and Wallrapp (1994). The subscript i , indicating the body
 467 index, is dropped. All quantities (vectors and matrices) are expressed in the body frame of reference; therefore, the prime notation is also
 468 dropped in this section. The number of flexible shape functions associated with the body is n_e , the flexible degrees of freedom are \mathbf{q}_e , and
 469 the shape functions are gathered into a matrix Φ of size $(3 \times n_e)$. The equations of motion, given in Equation 11, are repeated below:

$$470 \begin{bmatrix} M_{xx} & M_{x\theta} & M_{xe} \\ & M_{\theta\theta} & M_{\theta e} \\ \text{sym.} & & M_{ee} \end{bmatrix} \begin{bmatrix} \mathbf{a}_i \\ \dot{\boldsymbol{\omega}}^i \\ \ddot{\mathbf{q}}_e \end{bmatrix} + \begin{bmatrix} \mathbf{k}_{\omega,x} \\ \mathbf{k}_{\omega,\theta} \\ \mathbf{k}_{\omega,e} \end{bmatrix} + \begin{bmatrix} 0 \\ 0 \\ \mathbf{k}_e \end{bmatrix} = \begin{bmatrix} \mathbf{f}_x \\ \mathbf{f}_\theta \\ \mathbf{f}_e \end{bmatrix} \quad (\text{A1})$$

471 The different terms of the mass matrix are obtained as follows:

$$472 \quad \mathbf{M}_{xx} = \int \mathbf{I}_3 \, dm = M \mathbf{I}_3 \quad (3 \times 3) \quad (\text{A2})$$

$$473 \quad \mathbf{M}_{x\theta} = - \int \tilde{\mathbf{s}}_P \, dm = -M \tilde{\mathbf{s}}_{CM} \quad (3 \times 3) \quad (\text{A3})$$

$$474 \quad \mathbf{M}_{\theta\theta} = - \int \tilde{\mathbf{s}}_P \tilde{\mathbf{s}}_P \, dm = \mathbf{J} \quad (3 \times 3) \quad (\text{A4})$$

$$475 \quad \mathbf{M}_{\theta e} = \int \tilde{\mathbf{s}}_P \Phi \, dm = \mathbf{C}_r^T \quad (3 \times n_e) \quad (\text{A5})$$

$$476 \quad \mathbf{M}_{xe} = \int \Phi \, dm = \mathbf{C}_t^T \quad (3 \times n_e) \quad (\text{A6})$$

$$477 \quad \mathbf{M}_{ee} = \int \Phi^T \Phi \, dm \quad (n_e \times n_e) \quad (\text{A7})$$

478 The integrals are volume integrals over the volume of the body (for beams, they reduce to line integrals). The notation $[\tilde{\cdot}]$ represents the skew
479 symmetric matrix. M is the mass of the body. The vector \mathbf{s}_{CM} is the vector from the origin of the body to undeflected center of mass (CM)
480 of the body. The notations \mathbf{C}_t ($n_e \times 3$) and \mathbf{C}_r ($n_e \times 3$) are introduced to match Wallrapp's notations. The vector \mathbf{s}_P is the vector from
481 the origin of the body to a deflected point of the body of elementary mass dm . The undeflected position of this point is written as \mathbf{s}_{P_0} and
482 the displacement field \mathbf{u} , such that: $\mathbf{s}_P = \mathbf{s}_{P_0} + \mathbf{u}$. Typically, the displacement field is given by $\mathbf{u} = \Phi \mathbf{q}_e$, but a higher-order expansion can
483 also be introduced (see Wallrapp (1994) and Appendix D4). Wallrapp also includes the elementary mass moment of inertia, which results in
484 additional terms in the integrals (see Wallrapp (1994)). Such contributions are relevant, for instance, when considering the torsion of a beam
485 (see Branlard (2019)). The block matrices \mathbf{M}_{xx} , \mathbf{M}_{xe} , and \mathbf{M}_{ee} do not depend on the deformation of the body and are therefore constant.
486 The other terms are functions of \mathbf{q}_e . They may be expressed as linear combinations of constant integrals (see Appendix D3).

487 The quadratic velocity terms, \mathbf{k}_ω , are given as:

$$488 \quad \mathbf{k}_{\omega,x} = 2\tilde{\omega} \mathbf{C}_t^T \dot{\mathbf{q}}_e + M \tilde{\omega} \tilde{\omega} \mathbf{s}_{CM} \quad (3 \times 1) \quad (\text{A8})$$

$$489 \quad \mathbf{k}_{\omega,\theta} = \tilde{\omega} \mathbf{M}_{\theta\theta} \omega + \left[\sum_{j=1..n_e} \mathbf{G}_{r,j} \dot{q}_{e,j} \right] \omega \quad (3 \times 1) \quad (\text{A9})$$

$$490 \quad \mathbf{k}_{\omega,e} = \left[\omega^T \mathbf{O}_{e,j} \omega \right]_{j=1..n_e} + \left[\sum_{j=1..n_e} \mathbf{G}_{e,j} \dot{q}_{e,j} \right] \omega \quad (n_e \times 1) \quad (\text{A10})$$

491 where

$$492 \quad \mathbf{G}_{r,j} = -2 \int \tilde{\mathbf{s}}_P \tilde{\Phi}_j \, dm \quad (3 \times 3) \quad (\text{A11})$$

$$493 \quad \mathbf{O}_{e,j} = \int \tilde{\Phi}_j \tilde{\mathbf{s}}_P \, dm = -\frac{1}{2} \mathbf{G}_{r,j}^T \quad (3 \times 3) \quad (\text{A12})$$

$$494 \quad \mathbf{G}_{e,j} = -2 \int \Phi^T \tilde{\Phi}_j \, dm \quad (n_e \times 3) \quad (\text{A13})$$

495 The first term of Equation A10 is obtained by vertically stacking the contribution of each shape function. In the standard input data format,
496 this term is reshaped as the product $\mathbf{O}_e \Omega$, where:

$$497 \quad \mathbf{O}_e = [O_{e,j,11}, O_{e,j,22}, O_{e,j,33}, O_{e,j,12} + O_{e,j,21}, O_{e,j,23} + O_{e,j,32}, O_{e,j,13} + O_{e,j,31}]_{j=1..n_e} \quad (n_e \times 6) \quad (\text{A14})$$

$$498 \quad \Omega = [\omega_x^2, \omega_y^2, \omega_z^2, \omega_x \omega_y, \omega_y \omega_z, \omega_x \omega_z] \quad (6 \times 1) \quad (\text{A15})$$

499 The body elastic forces are given by:

$$500 \quad \mathbf{k}_e = \mathbf{k}_\sigma + \mathbf{K}_e \mathbf{q}_e + \mathbf{D}_e \dot{\mathbf{q}}_e \quad (\text{A16})$$

501 where \mathbf{K}_e and \mathbf{D}_e are the elastic stiffness and damping matrices, and \mathbf{k}_σ represents geometric stiffening terms (see Appendix C). The elastic
502 damping forces are often given as stiffness proportional damping. For more details, see Wallrapp (1994), and for more examples with elastic
503 beams, see Branlard (2019). The external loads can be assumed to consist of distributed volume forces, \mathbf{p} (in practice they are primarily
504 surface forces or line forces), and a gravitational acceleration field, \mathbf{g} . The components of the external loads in Equation A1 are then obtained
505 by integration over the whole body:

$$506 \quad \mathbf{f}_x = \int \mathbf{p} dV + \mathbf{M}_{xx} \mathbf{g} \quad (3 \times 1) \quad (\text{A17})$$

$$507 \quad \mathbf{f}_\theta = \int \mathbf{s}_P \times \mathbf{p} dV + \mathbf{M}_{\theta x} \mathbf{g} \quad (3 \times 1) \quad (\text{A18})$$

$$508 \quad \mathbf{f}_e = \int \Phi^T \mathbf{p} dV + \mathbf{M}_{ex} \mathbf{g} \quad (n_e \times 1) \quad (\text{A19})$$

509 Appendix B: Application of the shape function approach to an isolated beam

510 In this section, we illustrate how the elastic equations of Appendix A can be applied to an isolated beam. Examples of applications are further
511 given in subsection 4.3 and subsection 4.4. We consider a beam directed along the z -axis and bending in the x and y directions. Expressions
512 are written in the coordinate system of the beam and primes are dropped in this section. The beam properties are the following: length, L ,
513 mass per length, m , and bending stiffness, EI_x and EI_y . We assume that the displacement field is such that the shape functions are functions
514 of z only: $\mathbf{u}(z, t) = \sum_{i=1}^{n_e} \Phi_i(z) \mathbf{q}_{e,i}(t)$. We also assume that the shape functions satisfy at least the geometric boundary conditions. The
515 kinetic energy of the beam is $T = \frac{1}{2} \int_0^L m \dot{\mathbf{u}}^2 dz = \frac{1}{2} \sum_i \sum_j M_{e,ij} \dot{\mathbf{q}}_{e,i} \dot{\mathbf{q}}_{e,i}$. where $M_{e,ij}$ is (see Equation A7):

$$516 \quad M_{e,ij} = \int_0^L m(z) \Phi_i(z) \cdot \Phi_j(z) dz, \quad i, j = 1, \dots, n_e \quad (\text{B1})$$

517 Equation B1 involves a scalar product of the shape functions at each spanwise position. Integrals over the moment of inertia can be used
518 to account for torsion (see Branlard (2019)). The potential energy (strain energy) of the beam, is obtained as $V = \frac{1}{2} \sum_i \sum_j K_{e,ij} \mathbf{q}_{e,i} \mathbf{q}_{e,j}$,
519 where $K_{e,ij}$ are the elements of the stiffness matrix, which, under the assumption of small deformations, are given by:

$$520 \quad K_{e,ij} = \int_0^L \left[EI_y \frac{d^2 \Phi_{i,x}}{dz^2} \frac{d^2 \Phi_{j,x}}{dz^2} + EI_x \frac{d^2 \Phi_{i,y}}{dz^2} \frac{d^2 \Phi_{j,y}}{dz^2} \right] dz, \quad i, j = 1, \dots, n_e \quad (\text{B2})$$

521 Elongation and torsional strains (EA and GK_t) can similarly be added to the strain energy and the stiffness matrix if longitudinal and
522 torsional displacement fields are included in the shape functions. The external loads on the beam are assumed to consist of a distributed force
523 vector, $\mathbf{p}(z)$. The virtual work done by the force \mathbf{p} for each virtual displacement $\delta \mathbf{q}_{e,i}$ provides the generalized force as (see Equation A17):

$$524 \quad f_{e,i} = \int_0^L \Phi_i \cdot \mathbf{p} dz \quad (\text{B3})$$

525 The equations of motion of the isolated beam and then written in matrix form as:

$$526 \quad \mathbf{M}_e \ddot{\mathbf{q}}_e + \mathbf{D}_e \dot{\mathbf{q}}_e + \mathbf{K}_e \mathbf{q}_e = \mathbf{f}_e \quad (\text{B4})$$

527 where $\mathbf{q}_e = [q_{e,1}, \dots, q_{e,n}]$. Damping is typically added a posteriori to the equations, where the Rayleigh damping assumption is often used:
528 $\mathbf{D}_e = \alpha \mathbf{M}_e + \beta \mathbf{K}_e$ (stiffness proportional damping implies $\alpha = 0$). If the shape functions are mode shapes, then the shape functions are
529 orthogonal, the mass and stiffness matrices are diagonal, and the stiffness values would be $K_{e,ii} = \omega_{e,i}^2 M_{e,ii}$, with $\omega_{e,i} = \sqrt{K_{e,ii}/M_{e,ii}}$
530 the eigenfrequency of the beam mode i . The modal damping is then given by $D_{e,ii} = 2\zeta_i M_{e,ii} \omega_{e,i}$, where ζ_i is the damping ratio associated
531 with mode i .

532 If the beam is loaded axially by a force $N(z)$, then this force produces a distributed load in the transverse direction equal to $\mathbf{n} =$
533 $\frac{\partial}{\partial z} [N(z) \frac{\partial \mathbf{u}}{\partial z}]$, with components in the y and z directions (see Branlard (2019)). The generalized force associated with this loading is then
534 $Q_{N,i} = \int_0^L \Phi_i \cdot \mathbf{n} dz$. Inserting the expression of \mathbf{n} and \mathbf{u} , the generalized force has the form of a stiffness term: $Q_{N,i} = -\sum_j K_{N,ij} q_j$ with

$$535 \quad K_{N,ij} = -\int_0^L \Phi_i \cdot \frac{d}{dz} \left[N(z) \frac{d\Phi_j}{dz} \right] dz = \int_0^L N(z) \frac{d\Phi_i}{dz} \cdot \frac{d\Phi_j}{dz} - \left[N(x) \Phi_i \cdot \frac{d\Phi_j}{dz} \right]_0^L \quad (\text{B5})$$

536 and where integration by parts was used to obtain the second equality. Examples of applications are given in subsection 4.3 and subsection 4.4.
537 The fact that an axial load leads to a stiffness term is referred to as “geometric stiffness,” which is the topic of Appendix C.

538 Appendix C: Geometric stiffness

539 C1 General treatment

540 Geometric stiffness refers to the apparent change of stiffness of a structure depending on the loading it is subject to. In this section, we present
541 a linear formulation of geometric stiffness for a flexible body undergoing motion and subject to arbitrary loading, inspired by Schwertassek
542 and Wallrapp (1999). Additional details may be found in Wallrapp and Schwertassek (1991). The main component of the geometric stiffening
543 term \mathbf{k}_σ can be written:

$$544 \quad \mathbf{k}_\sigma = \mathbf{K}_g \mathbf{q}_e \quad (\text{C1})$$

545 where \mathbf{K}_g is the geometric stiffness matrix of shape $n_e \times n_e$. In general, this matrix is time-dependent, as it is a function of the inertial and
546 external loads acting on the body. The inertial loads consist of contributions from the linear acceleration, \mathbf{a} , rotational acceleration, $\dot{\boldsymbol{\omega}}$, and
547 cross products of the rotational velocity of the body (centrifugal and gyroscopic terms). The external loads consist of the gravitational force,
548 distributed forces per unit length, \mathbf{p} , point loads, \mathbf{F}^k , and point moments, $\boldsymbol{\tau}^k$, where k is the node index where the point loads are applied.
549 Each of these contributions can be computed at each time step using a linear superposition of unit geometric stiffness matrices, noted \mathbf{K}_{g*} ,
550 as follows:

$$551 \quad \mathbf{K}_g = \sum_{\alpha=1}^3 [(a_\alpha - g_\alpha) \mathbf{K}_{gt,\alpha} + \dot{\omega}_\alpha \mathbf{K}_{gr,\alpha}] + \sum_{\alpha=1}^3 \sum_{\beta=1}^3 \omega_\alpha \omega_\beta \mathbf{K}_{g\omega,\alpha\beta}$$

$$552 \quad + \sum_{\alpha=1}^3 \left[p_\alpha \mathbf{K}_{gp,\alpha} + \sum_k \left(F_\alpha^k \mathbf{K}_{gF,\alpha}^k + \tau_\alpha^k \mathbf{K}_{g\tau,\alpha}^k \right) \right] \quad (\text{C2})$$

553 where the indices α and β run on the x, y , and z coordinates of the body reference frame. The matrices $\mathbf{K}_{g*,\alpha}$ or $\mathbf{K}_{g*,\alpha\beta}$ have the shape
554 $n_e \times n_e$ and are obtained as the geometric stiffness matrices for unit accelerations, loads, or products of rotational velocities in the given
555 direction defined by α and β (x, y , or z). For instance, $\mathbf{K}_{gt,z}$ is the geometric stiffness matrix corresponding to a unit acceleration in the z
556 direction, $\mathbf{K}_{g\omega,xy}^k$ is the geometric stiffness matrix corresponding to a unit gyration about the x and y directions, and $\mathbf{K}_{gF,\alpha}^k$ is the geometric

557 stiffness matrix corresponding to a unit force in the x direction applied at the node k along the body. We note that the terms \mathbf{K}_{g*} have
 558 different units; for instance, the terms $\mathbf{K}_{gt,*}$ are expressed in $\text{N} \cdot \text{s}^2 \cdot \text{m}^{-2}$.

559 C2 Expressions for a beam directed along z

560 The expression for each of these matrices are given in Schwertassek and Wallrapp (1999) in the context of the finite-element method. The
 561 general expressions for a shape function approach would be beyond the scope of this article, but we provide the expressions for a beam
 562 below.

563 We adopt the same notations as Appendix B to describe the flexible beam. The different unit geometric matrices introduced in Appendix C
 564 can be determined using a form of Equation B5, where the axial load N is replaced by the unit inertial or external load. Since the beam is
 565 directed along the z direction, we focus on the terms where the loads act in the z direction, all other terms being zero or negligible. The
 566 ij -component of the matrix $\mathbf{K}_{gt,z}$ is obtained by considering a unit vertical acceleration:

$$567 \quad K_{gt,z,ij} = \int_0^L N(z) \frac{d\Phi_i}{dz} \cdot \frac{d\Phi_j}{dz} dz, \quad N(z) = \int_z^L m(z) dz \quad (\text{C3})$$

568 We write z_k the coordinate of node k along the beam. The ij -component of the matrix $\mathbf{K}_{gF,z}^k$ is obtained as:

$$569 \quad K_{gF,z,ij}^k = \int_0^L N(z) \frac{d\Phi_i}{dz} \cdot \frac{d\Phi_j}{dz} dz, \quad N(z) = 1 \text{ if } z < z_k, 0 \text{ otherwise} \quad (\text{C4})$$

570 The ij -component of the matrix $\mathbf{K}_{g\omega,\alpha\beta}$ is obtained by considering unit centrifugal loads generated using independent rotations around the
 571 unit vectors \mathbf{e}_x , \mathbf{e}_y , and \mathbf{e}_z :

$$572 \quad K_{g\omega,\alpha\beta,ij} = \int_0^L -\mathbf{e}_z \cdot (\tilde{\mathbf{e}}_\alpha \tilde{\mathbf{e}}_\beta \mathbf{N}(z)) \frac{d\Phi_i}{dz} \cdot \frac{d\Phi_j}{dz} dz, \quad \mathbf{N}(z) = \int_z^L m(z) \mathbf{s}_{P_0} dz \quad (\text{C5})$$

573 Similarly, the ij -component of the matrix $\mathbf{K}_{gr,\alpha}$ is:

$$574 \quad K_{gr,\alpha,ij} = \int_0^L -\mathbf{e}_z \cdot (\tilde{\mathbf{e}}_\alpha \mathbf{N}(z)) \frac{d\Phi_i}{dz} \cdot \frac{d\Phi_j}{dz} dz, \quad \mathbf{N}(z) = \int_z^L m(z) \mathbf{s}_{P_0} dz \quad (\text{C6})$$

575 C3 Integration into the equations of motion

576 The term $\mathbf{k}_\sigma = \mathbf{K}_g \mathbf{q}_e$ appears on the third block-row of the equations of motion of the flexible body (Equation A1). Because of the linearity
 577 with respect to the acceleration, rotational velocities, and forces, the different contributions can optionally be incorporated into the third
 578 block-row of the mass matrix (\mathbf{M}_{e*}), the term $\mathbf{k}_{\omega,e}$, and the term \mathbf{f}_e , respectively. For instance, the term $\sum a_\alpha \mathbf{K}_{gt,\alpha} \mathbf{q}_e$ can be reorganized
 579 as $[\mathbf{K}_{gt}] \mathbf{q}_e \cdot \mathbf{a}$ (using loose notations); therefore, the mass matrix can be updated such that \mathbf{M}_{xe} becomes $\mathbf{M}_{xe} + [\mathbf{K}_{gt}] \mathbf{q}_e$. When a Taylor
 580 expansion is used, such integration is easily implemented as a first-order term (see Appendix D3).

581 Appendix D: Alternative formulations

582 Different formulations of flexible multibody dynamics using shape functions are found in the literature. Some of the alternatives are briefly
 583 discussed in this section.

584 D1 Jacobian and velocity transformation matrix

585 In Equation 7, the Jacobian terms \mathbf{J} and the virtual work are expressed in vector form. In such form, there is no need to state in which coordi-
 586 nate system the different vectors are expressed. This is convenient to reduce the size of the expressions when using symbolic calculations. In
 587 a numerical framework, the vector will have to be expressed in a common frame. When such an approach is used (see, e.g., Lemmer (2018);
 588 Branlard (2019)), the Jacobians are sometimes stacked into a matrix form:

$$589 \mathbf{J} = \begin{bmatrix} \mathbf{J}_v \\ \mathbf{J}_\omega \\ \mathbf{J}_e \end{bmatrix} \quad (D1)$$

590 Some implementation choices are needed depending if these matrices are expressed in the global frame or a body frame. The Jacobian
 591 matrices are referred to as “velocity transformation matrix,” and the link between formulations in global and local coordinates is given in
 592 Branlard (2019). In the same reference, recursive relationships are given for tree-like assembly of bodies to help express the Jacobian matrices
 593 of each body recursively, based on the matrices of the parent body. It is also noted that the quadratic velocity terms, \mathbf{k}_ω , can be obtained
 594 using the time derivative of the Jacobian matrix.

595 D2 Rotations and torsion

596 In this article, we have not elaborated on the change of orientation introduced by shape functions. In most applications, bodies are connected
 597 at their extremities and the deflection slope at a body extremity will induce a rotation of the subsequent body (e.g., tilting and rolling of
 598 the nacelle at the tower top). The deflection slope can be obtained from the knowledge of the shape functions. This is readily accounted
 599 for by introducing a time-varying rotation matrix between bodies, and this is the approach used in our symbolic framework. A formalism
 600 of rotations of bodies connected at their extremities is given in Branlard (2019). A more general formulation, introducing shape function
 601 rotations Ψ , is given in (Wallrapp, 1994; Schwertassek and Wallrapp, 1999; Lemmer, 2018). In such a formulation, the linear rotation field
 602 is obtained as $\mathbf{I} + \widetilde{\Psi}\mathbf{q}$, where \mathbf{I} is the identity matrix.

603 D3 Shape integrals and Taylor expansion

604 The results presented in Appendix A consist of integrals over the displaced points of the structure, $\mathbf{s}_P = \mathbf{s}_{P_0} + \mathbf{u}$, where the displacement
 605 field is $\mathbf{u} = \Phi\mathbf{q}_e$. The undeflected position of the structure (\mathbf{s}_{P_0}) is constant, and the shape functions are known at the initialization; the only
 606 time-varying terms are the degrees of freedom \mathbf{q}_e . Therefore, the integrals can be precomputed by decomposing them into a constant part
 607 and a part that is linear with respect to the degrees of freedom \mathbf{q}_e . The precomputed integrals are referred to as “shape integrals.” For a given
 608 term \mathbf{T} (standing, for instance, for $\mathbf{M}_{\theta,\theta}$, \mathbf{C}_t , \mathbf{C}_r , \mathbf{G}_r , \mathbf{G}_e , or \mathbf{O}_e), the shape integral expansion is:

$$609 \mathbf{T}(\mathbf{q}_e) = \mathbf{T}^0 + \sum_{j=1..n_e} \mathbf{T}_j^1 q_{e,j} \quad (D2)$$

610 If \mathbf{T} is an array, \mathbf{T}^0 and \mathbf{T}_j^1 have the same shape as \mathbf{T} . As an example, the application of the shape integral expansion to the term $\mathbf{M}_{x\theta}$ (see
 611 Equation A3) gives:

$$612 \mathbf{M}_{x\theta} = - \int \tilde{\mathbf{s}}_P dm = \mathbf{M}_{x\theta}^0 + \sum_{j=1..n_e} \mathbf{M}_{x\theta,j}^1 q_{e,j} \quad (D3)$$

613 with

$$614 \quad M_{x\theta}^0 = - \int \tilde{s}_{P_0} dm, \quad M_{x\theta,j}^1 = - \int \tilde{\Phi}_j dm \quad (D4)$$

615 The zeroth- and first-order shape integrals always consist of integrals over the components of s_{P_0} and Φ , which can be precomputed for a
 616 given flexible body. We note that the precomputed shape integrals can in turn be obtained from intermediate integrals (e.g., the S_* and N_*
 617 terms introduced by Wallrapp (Wallrapp, 1994), or the σ , Σ , Υ , Ψ terms introduced by Shabana (Shabana, 2013)). The zeroth- and first-order
 618 shape integrals are stored using a ‘‘Taylor’’ object-oriented class in the standard input data format defined by Wallrapp. The YAMS library
 619 can compute the shape integrals using a direct integration or using a finite-element formulation (see Schwertassek and Wallrapp (1999)).

620 The geometric stiffness introduced in Appendix C is linear in the elastic degrees of freedom q_e . Therefore, the unit geometric stiffness
 621 matrices (which are also shape integrals) can be conveniently added into the first-order terms of Equation D2. For instance, if we write M_{ex}
 622 (given in Equation A6) using a first-order expansion, $M_{ex} = M_{ex}^0 + M_{ex}^1 q_e$, then the geometric stiffening effect can directly be inserted
 623 into the first-order term, such that M_{ex}^1 becomes $M_{ex}^1 + K_{gt}$. Similarly, the term K_{gr} can be inserted into $M_{\theta e}^1$, $K_{g\omega}$ into O_e^1 , K_{gF} into
 624 Φ^1 , and $K_{g\tau}$ into Ψ^1 in the calculation of the generalized forces. The different contributions are summarized in Table 6.9 of the book of
 625 Schwertassek and Wallrapp (1999). A shortcoming of inserting the geometric stiffness effects into the first-order coefficient is that it could
 626 make the mass matrix symmetric (if the user code assumes $M_{xe} = M_{ex}^t$), instead of acting only on the third block-row of the mass matrix.

627 **D4 Taylor expansion of the displacement field**

628 In the work of Wallrap (Wallrapp, 1993, 1994), the displacement field is assumed to be a function of the degrees of freedom, $u = \Phi_u(q_e)q_e$,
 629 where Φ_u consists of a Taylor series expansion of the shape functions that contain Φ^0 and Φ^1 terms. The resulting equations of motion are
 630 still expressed using shape integrals of the form given in Equation D2, but the 1 terms will contain some additional integrals over Φ^1 . The
 631 advantage of this method is that the Φ^1 terms effectively account for the geometric stiffness. In practice, it is equivalent, and as convenient,
 632 to neglect the Φ^1 terms and introduce the geometric stiffness using the method presented in Appendix C (and optionally integrate them into
 633 the 1 terms as presented in Appendix D3).

634 **D5 ElastoDyn and the partial loads approach**

635 The ElastoDyn module of OpenFAST (Jonkman et al., 2021) uses the so-called ‘‘partial loads’’ approach to implement the equations of
 636 motion. The underlying theory used to derive the equations of motion is the same as Kane’s formalism presented in section 2, but the partial
 637 load approach takes advantage of the fact that the calculation of reaction loads or point loads at body extremities requires similar terms to the
 638 ones needed for the equations of motion. In the discussion below, we assume that the different bodies of the structure form a tree structure
 639 with the root at the bottom and the leaves above. For a tree-like structure, there is a natural relationship between loads in the structure and the
 640 degrees of freedom. A virtual displacement of a given degree of freedom will only displace the structure above it. The equation of motion
 641 of this degree of freedom can therefore be obtained from the virtual work of the loads at a point located just above the degree of freedom,
 642 as if the entire structure above was replaced by lumped loads. The point loads contain contributions from the external loads above the point
 643 in consideration, but also inertial and gyroscopic loads associated with all the degrees of freedom of the system. If the point is at a joint, the
 644 loads corresponds to the reaction loads at this point. We write P the point located after a given degree of freedom r . The equation of motion
 645 for this degree of freedom is obtained as if the system was isolated:

$$646 \quad \dot{f}_r + \dot{f}_r^* = 0 = J_{vP,r} \cdot f_P + J_{\omega P,r} \cdot \tau_P + h_r \quad (D5)$$

647 where: $\mathbf{J}_{v_{P,r}}$ and $\mathbf{J}_{\omega_{P,r}}$ are the partial velocities of point P with respect to the degree of freedom r ; \mathbf{f}_P and $\boldsymbol{\tau}_P$ are 3-vectors containing the
648 force and torque from the structure above the degree of freedom r (including external and inertial contributions); and h_r is the generalized
649 load associated with the isolated degree of freedom r (e.g., the elastic loads for a flexible body, or the spring and damping loads for a degree
650 of freedom representing a joint). The point loads \mathbf{f}_P and $\boldsymbol{\tau}_P$ can be decomposed into terms that are proportional to the accelerations of all
651 the degrees of freedom (indexed with r) and additional terms (labeled “ t ”):

$$652 \quad \mathbf{f}_P = \sum_{j=1}^{n_q} \mathbf{f}_{P,j} \ddot{q}_j + \mathbf{f}_{P,t}, \quad \boldsymbol{\tau}_P = \sum_{j=1}^{n_q} \boldsymbol{\tau}_{P,j} \ddot{q}_j + \boldsymbol{\tau}_{P,t} \quad (D6)$$

653 The terms $\mathbf{f}_{P,r}$ and $\boldsymbol{\tau}_{P,r}$ act as generalized masses and they are referred to as “partial loads”. Combining Equation D5 and Equation D6, the
654 term rj of the mass matrix and the term r of the right hand side of the equation of motion (Equation 22) are obtained as:

$$655 \quad M_{rj} = -\mathbf{J}_{v_{P,r}} \cdot \mathbf{f}_{P,j} - \mathbf{J}_{\omega_{P,r}} \cdot \boldsymbol{\tau}_{P,j}, \quad F_r = \mathbf{J}_{v_{P,r}} \cdot \mathbf{f}_{P,t} + \mathbf{J}_{\omega_{P,r}} \cdot \boldsymbol{\tau}_{P,t} + h_r \quad (D7)$$

656 Therefore, the knowledge of the partial loads and the partial velocities at key points of the structure (typically, points where user outputs
657 are desired) can be used to obtain the reaction loads (Equation D6) and the equations of motion (Equation D7). This is the approach used
658 in ElastoDyn: the loads at key points of the structure were derived using hand calculations, and then the partial loads were used for the
659 implementation of the outputs and the equations of motion. The reader is referred to the notes provided in the online documentation of
660 ElastoDyn for more details (Jonkman et al., 2021). A general procedure to obtain partial loads can be devised (using kinematics to find
661 velocities and acceleration in the structure, and computing the loads from the tree top to the root), but would be beyond the scope of this
662 article.

663 Appendix E: Equations of motion of simple wind turbine models

664 In this section, we present the equations of motion for the examples presented in section 4.

665 E1 Two-degrees-of-freedom model of a land-based or fixed-bottom wind turbine

666 In this section, we provide some intermediate values to obtain the equations of motion given in subsection 4.4. We use the hat notation to
667 indicate unit vectors of a frame, where the frame is identified as t , n , r for the tower, nacelle, and rotor, respectively. For instance, $v\hat{t}_x$ is the
668 unit vector in the x direction of the tower frame. The degrees of freedom are $\mathbf{q} = (q, \psi)$. The kinematics of the tower (at its origin) are zero:

$$669 \quad \mathbf{v}_{O,T} = \mathbf{0}, \quad \boldsymbol{\omega}_T = \mathbf{0}, \quad \mathbf{a}_{O,T} = \mathbf{0} \quad (E1)$$

670 All Jacobians are zero except $\mathbf{J}_{e,1T} = 1$ The inertial force, torque, and elastic force are:

$$671 \quad \mathbf{f}_T^* = C_{tTx} \ddot{q} \hat{\mathbf{t}}_x + M_T g \hat{\mathbf{t}}_z, \quad \boldsymbol{\tau}_T^* = C_{rTy} \ddot{q} \hat{\mathbf{t}}_y, \quad \mathbf{E}_T^* = f_e + D_e \dot{q} + (K_e + K_q)q + M_e \ddot{q} \quad (E2)$$

672 The nacelle kinematics (at its center of mass) are:

$$673 \quad \mathbf{v}_{G,N} = \dot{q} \hat{\mathbf{t}}_x + \nu_y z_{NG} \dot{q} \hat{\mathbf{n}}_x - \nu_y x_{NG} \dot{q} \hat{\mathbf{n}}_z, \quad \boldsymbol{\omega}_N = \nu_y \dot{q} \hat{\mathbf{t}}_y \quad (E3)$$

$$674 \quad \mathbf{a}_{G,N} = \ddot{q} \hat{\mathbf{t}}_x + (-\nu_y^2 x_{NG} \dot{q}^2 + \nu_y z_{NG} \ddot{q}) \hat{\mathbf{n}}_x + (-\nu_y^2 z_{NG} \dot{q}^2 - \nu_y x_{NG} \ddot{q}) \hat{\mathbf{n}}_z \quad (E4)$$

675 The Jacobians with respect to q are:

$$676 \quad \mathbf{J}_{v,1N} = \hat{\mathbf{t}}_x + \nu_y z_{NG} \hat{\mathbf{n}}_x - \nu_y x_{NG} \hat{\mathbf{n}}_z, \quad \mathbf{J}_{\omega,1N} = \nu_y \hat{\mathbf{t}}_y \quad (E5)$$

677 The inertial force and torque on the nacelle are:

$$678 \quad \mathbf{f}_N^* = M_N \ddot{q} \hat{\mathbf{t}}_x + M_N (-\nu_y^2 x_{NG} \dot{q}^2 + \nu_y z_{NG} \ddot{q}) \hat{\mathbf{n}}_x + M_N (-\nu_y^2 z_{NG} \dot{q}^2 - \nu_y x_{NG} \ddot{q}) \hat{\mathbf{n}}_z, \quad \boldsymbol{\tau}_N^* = J_{y,N} \nu_y \ddot{q} \hat{\mathbf{n}}_y \quad (\text{E6})$$

679 The kinematics of the rotor are:

$$680 \quad \mathbf{v}_{G,R} = \dot{q} \hat{\mathbf{t}}_x + \nu_y z_{NR} \dot{q} \hat{\mathbf{n}}_x - \nu_y x_{NR} \dot{q} \hat{\mathbf{n}}_z, \quad \boldsymbol{\omega}_R = \dot{\psi} \hat{\mathbf{e}}_{\mathbf{r}\mathbf{x}} + \nu_y \dot{q} \hat{\mathbf{t}}_y \quad (\text{E7})$$

$$681 \quad \mathbf{a}_{G,R} = \ddot{q} \hat{\mathbf{t}}_x + (-\nu_y^2 x_{NR} \dot{q}^2 + \nu_y z_{NR} \ddot{q}) \hat{\mathbf{n}}_x + (-\nu_y^2 z_{NR} \dot{q}^2 - \nu_y x_{NR} \ddot{q}) \hat{\mathbf{n}}_z \quad (\text{E8})$$

682 The corresponding Jacobians with respect to q (“1”) and ψ (“2”) are:

$$683 \quad \mathbf{J}_{v,1R} = \hat{\mathbf{t}}_x + \nu_y z_{NR} \hat{\mathbf{n}}_x - \nu_y x_{NR} \hat{\mathbf{n}}_z, \quad \mathbf{J}_{\omega,1R} = \nu_y \hat{\mathbf{t}}_y, \quad \mathbf{J}_{\omega,2R} = \hat{\mathbf{r}}_x$$

684 The inertial force and torque on the rotor are:

$$685 \quad \mathbf{f}_R^* = M_R \ddot{q} \hat{\mathbf{t}}_x + M_R (-\nu_y^2 x_{NR} \dot{q}^2 + \nu_y z_{NR} \ddot{q}) \hat{\mathbf{n}}_x + M_R (-\nu_y^2 z_{NR} \dot{q}^2 - \nu_y x_{NR} \ddot{q}) \hat{\mathbf{n}}_z \quad (\text{E9})$$

$$686 \quad \boldsymbol{\tau}_R^* = J_{x,R} \ddot{\psi} \hat{\mathbf{r}}_x \quad (\text{E10})$$

$$687 \quad + (J_{\oplus,R} \nu_y \sin(\psi) \dot{\psi} \dot{q} + J_{\oplus,R} (-\nu_y \sin(\psi) \dot{\psi} \dot{q} + \nu_y \cos(\psi) \ddot{q}) - J_{x,R} \nu_y \sin(\psi) \dot{\psi} \dot{q}) \hat{\mathbf{r}}_y \quad (\text{E11})$$

$$688 \quad + (J_{\oplus,R} \nu_y \cos(\psi) \dot{\psi} \dot{q} + J_{\oplus,R} (-\nu_y \sin(\psi) \ddot{q} - \nu_y \cos(\psi) \dot{\psi} \dot{q}) - J_{x,R} \nu_y \cos(\psi) \dot{\psi} \dot{q}) \hat{\mathbf{r}}_z \quad (\text{E12})$$

689 E2 Three-degrees-of-freedom model of a land-based or fixed-bottom wind turbine

690 The equations of motion for the model presented in subsection 4.5, with $\mathbf{q} = (q_1, q_2, \psi)$, are given in this section. The elements of the mass
691 matrix are:

$$692 \quad M_{11} = [M_{e11} + M_N + M_R] \quad (\text{E13})$$

$$693 \quad + [J_{y,N} + J_{\oplus,R} + M_N (x_{NG}^2 - 2x_{NG}q_1 + z_{NG}^2) + M_R (x_{NR}^2 - 2x_{NR}q_1 + z_{NR}^2)] \nu_y^2 \quad (\text{E14})$$

$$694 \quad + 2[M_N z_{NG} + M_R z_{NR}] \nu_y \quad (\text{E15})$$

$$695 \quad M_{13} = J_{x,R} \theta_t \nu_x \nu_y q_2 \quad (\text{E16})$$

$$696 \quad M_{22} = [M_{e22} + M_N + M_R] \quad (\text{E17})$$

$$697 \quad + [J_{x,N} + J_{x,R} + M_N z_{NG}^2 + M_R z_{NR}^2] \nu_x^2 \quad (\text{E18})$$

$$698 \quad - 2[M_N z_{NG} + M_R z_{NR}] \nu_x \quad (\text{E19})$$

$$699 \quad M_{23} = J_{x,R} \nu_x \quad (\text{E20})$$

$$700 \quad M_{33} = J_{x,R} \quad (\text{E21})$$

701 The elements of the forcing vector are:

$$702 \quad f_1 = f_{e1} - K_{e11} q_1 - D_{e11} \dot{q}_1 - J_{x,R} \theta_t \nu_x \nu_y \dot{\psi} \dot{q}_2 + [M_N x_{NG} + M_R x_{NR}] \nu_y^2 \dot{q}_1^2 \quad (\text{E22})$$

$$703 \quad + g [M_N (\nu_y^2 z_{NG} q_1 + \nu_y x_{NG}) + M_R (\nu_y^2 z_{NR} q_1 + \nu_y x_{NR})] + f_a [\theta_t \nu_y x_{NR} - \theta_t \nu_y q_1 + \nu_y z_{NR} + 1] \quad (\text{E23})$$

$$704 \quad f_2 = f_{e2} - K_{e22} q_2 - D_{e22} \dot{q}_2 + J_{x,R} \theta_t \nu_x \nu_y \dot{\psi} \dot{q}_1 \quad (\text{E24})$$

$$705 \quad + g [M_N z_{NG} + M_R z_{NR}] \nu_x^2 q_2 + f_a \theta_t \nu_x q_2 \quad (\text{E25})$$

$$706 \quad f_3 = -J_{x,R} \theta_t \nu_x \nu_y \dot{q}_1 \dot{q}_2 + \tau_a \quad (\text{E26})$$

707 E3 Three-degrees-of-freedom model of a floating wind turbine

708 The equations of motion for the model presented in subsection 4.6, with $\mathbf{q} = (x, \phi, q_T)$, are given in this section. The elements of the mass
709 matrix are:

$$710 \quad M_{11} = M_F + M_T + M_N \quad (\text{E27})$$

$$711 \quad M_{12} = M_F z_{FG} - M_{dz} + M_N [L_T + z_{NG} - \nu_y x_{NG} q_T - \phi_y (x_{NG} + q_T + \nu_y z_{NG} q_T)] \quad (\text{E28})$$

$$712 \quad M_{13} = C_{tT1x} + M_N [1 + \nu_y z_{NG} - \nu_y^2 x_{NG} q_T - \phi_y (\nu_y^2 z_{NG} q_T + \nu_y x_{NG})] \quad (\text{E29})$$

$$713 \quad M_{22} = J_{y,F} + M_F z_{FG}^2 + J_{T,y} + J_{y,N} + M_N [(L_T^2 + z_{NG})^2 + (q_T + x_{NG})^2 + 2\nu_y q_T (z_{NG} q_T - L_T x_{NG})] \quad (\text{E30})$$

$$714 \quad M_{23} = C_{rT1y} + [J_{y,N} + M_N (x_{NG}^2 + z_{NG}^2 + L_T z_{NG} + \nu_y q_T (z_{NG} q_T - L_T x_{NG}))] \nu_y + M_N [L_T + z_{NG}] \quad (\text{E31})$$

$$715 \quad M_{33} = M_e + M_N + [J_{y,N} + M_N (x_{NG}^2 - 2x_{NG} q_T + z_{NG}^2)] \nu_y^2 + 2M_N \nu_y z_{NG} \quad (\text{E32})$$

716 The elements of the forcing vector are:

$$717 \quad f_1 = f_H + [M_F z_{FG} - M_{dz} + M_N (L_T + z_{NG} - \nu_y x_{NG} q_T)] \phi_y \dot{\phi}_y^2 + M_N [q_T + x_{NG} + \nu_y z_{NG} q_T] \dot{\phi}_y^2 \quad (\text{E33})$$

$$718 \quad + [2C_{tx} + M_N (1 + \nu_y z_{NG} - \nu_y^2 x_{NG} q_T)] \phi_y \dot{\phi}_y \dot{q}_T + M_N \nu_y [x_{NG} + \nu_y z_{NG} q_T] \dot{\phi}_y \dot{q}_T \quad (\text{E34})$$

$$719 \quad + M_N \nu_y^2 [x_{NG} + z_{NG} \phi_y] \dot{q}_T^2 \quad (\text{E35})$$

$$720 \quad + f_a [1 - \theta_t \nu_y q_T - \nu_y \phi_y q_T] \quad (\text{E36})$$

$$721 \quad f_2 = \tau_H + M_N [\nu_y^2 (L_T x_{NG} - z_{NG} q_T)] \dot{q}_T^2 \quad (\text{E37})$$

$$722 \quad - 2M_N [q_T + x_{NG} + \nu_y (2z_{NG} q_T - L_T x_{NG}) - \nu_y^2 q_T (L_T z_{NG} + x_{NG} q_T)] \dot{\phi}_y \dot{q}_T \quad (\text{E38})$$

$$723 \quad + g [M_F z_{FG} \phi_y - M_{dz} \phi_y + M_N \{(L_T + z_{NG} - \nu_y x_{NG} q_T) \phi_y + q_T + x_{NG} + \nu_y z_{NG} q_T\}] \quad (\text{E39})$$

$$724 \quad + f_a [L_T + z_{NR} + \theta_t x_{NR} + \theta_t q_T + \nu_y q_T^2 - L_T \theta_t \nu_y q_T] \quad (\text{E40})$$

$$725 \quad f_3 = f_e - D_e \dot{q}_T - K_e q_T \quad (\text{E41})$$

$$726 \quad + M_N [q_T + x_{NG} + \nu_y (2z_{NG} q_T - L_T x_{NG}) - \nu_y^2 q_T (L_T z_{NG} + x_{NG} q_T)] \dot{\phi}_y^2 \quad (\text{E42})$$

$$727 \quad + M_N \nu_y^2 x_{NG} \dot{q}_T^2 \quad (\text{E43})$$

$$728 \quad + g [C_{tT1x} \phi_y + M_N (\nu_y x_{NG} + \nu_y^2 z_{NG} q_T - \nu_y^2 x_{NG} \phi_y q_T + \nu_y z_{NG} \phi_y + \phi_y)] \quad (\text{E44})$$

$$729 \quad + f_a [1 + \theta_t \nu_y x_{NR} - \theta_t \nu_y q_T + \nu_y z_{NR}] \quad (\text{E45})$$

730 **References**

- 731 ANSYS: <https://www.ansys.com/>, accessed: 2022-03-19, 2022.
- 732 Bauchau, O. A.: Flexible Multibody Dynamics, Solid Mechanics and Its Applications, Springer, Dordrecht, [https://doi.org/10.1007/978-94-](https://doi.org/10.1007/978-94-007-0335-3)
733 007-0335-3, 2011.
- 734 Bielawa, R.: Rotary wing structural dynamics and aeroelasticity, AIAA education series, American Institute of Aeronautics and Astronautics,
735 2006.
- 736 Branlard, E.: Flexible multibody dynamics using joint coordinates and the Rayleigh-Ritz approximation: The general framework behind and
737 beyond Flex, *Wind Energy*, 22, 877–893, <https://doi.org/10.1002/we.2327>, 2019.
- 738 Branlard, E.: WELIB, Wind Energy Library, GitHub repository <http://github.com/ebranlard/welib/>, 2021.
- 739 Branlard, E., Giardina, D., and Brown, C. S. D.: Augmented Kalman filter with a reduced mechanical model to estimate tower loads on
740 a land-based wind turbine: a step towards digital-twin simulations, *Wind Energy Science*, 5, 1155–1167, [https://doi.org/10.5194/wes-5-](https://doi.org/10.5194/wes-5-1155-2020)
741 1155-2020, 2020a.
- 742 Branlard, E., Jonkman, J., Dana, S., and Doubrawa, P.: A digital twin based on OpenFAST linearizations for real-time load and fatigue esti-
743 mation of land-based turbines, *Journal of Physics: Conference Series*, 1618, 022 030, <https://doi.org/10.1088/1742-6596/1618/2/022030>,
744 2020b.
- 745 Docquier, N., Poncelet, A., and Fisette, P.: ROBOTRAN: a powerful symbolic generator of multibody models, *Mech. Sci.*, 4, 199–219,
746 <https://doi.org/10.5194/ms-4-199-2013>, 2013.
- 747 Gede, G., Peterson, D., Nanjangud, A., Moore, J., and Hubbard, M.: Constrained Multibody Dynamics With Python: From Symbolic Equa-
748 tion Generation to Publication., in: *Proceedings of the ASME 2013 International Design Engineering Technical Conferences and Com-*
749 *puters and Information in Engineering Conference*. Portland, Oregon, USA. August 4-7, <https://doi.org/10.1115/DETC2013-13470>, 2013.
- 750 Geisler, J.: CADynTub: Wind Turbine Model from OpenFAST Data using CADyn Equations of Motion, [https://github.com/jgeisler0303/](https://github.com/jgeisler0303/CADynTurb)
751 CADynTurb, 2021.
- 752 G eradin, M. and Cardona, A.: Flexible Multibody Dynamics: A Finite Element Approach, Wiley, 2001.
- 753 Jeleni c, G. and Crisfield, M.: Geometrically exact 3D beam theory: implementation of a strain-invariant finite element for statics and dynam-
754 ics, *Computer Methods in Applied Mechanics and Engineering*, 171, 141–171, [https://doi.org/10.1016/S0045-7825\(98\)00249-7](https://doi.org/10.1016/S0045-7825(98)00249-7), 1999.
- 755 Jonkman, B., Mudafort, R. M., Platt, A., Branlard, E., Sprague, M., Jonkman, J., Vijayakumar, G., Buhl, M., Ross, H., Bortolotti, P., Masciola,
756 M., Ananthan, S., Schmidt, M. J., Rood, J., Damiani, R., Mendoza, N., Hall, M., and Corniglion, R.: OpenFAST v3.1.0. Open-source wind
757 turbine simulation tool, available at <http://github.com/OpenFAST/OpenFAST/>, <https://doi.org/10.5281/zenodo.6324288>, 2021.
- 758 Jonkman, J., Butterfield, S., Musial, W., and Scott, G.: Definition of a 5MW Reference Wind Turbine for Offshore System Development,
759 Tech. Rep. NREL/TP-500-38060, National Renewable Energy Laboratory, <https://doi.org/10.2172/947422>, 2009.
- 760 Jonkman, J. M.: Dynamics of offshore floating wind turbines—model development and verification, *Wind Energy*, 12, 459–492,
761 <https://doi.org/10.1002/we.347>, 2009.
- 762 Jonkman, J. M., Branlard, E., and Jasa, J. P.: Influence of wind turbine design parameters on linearized physics-based models in OpenFAST,
763 *Wind Energy Science*, 7, 559–571, <https://doi.org/10.5194/wes-7-559-2022>, 2022.
- 764 Kane, T. R. and Wang, C. F.: On the Derivation of Equations of Motion, *Journal of the Society for Industrial and Applied Mathematics*, 13,
765 487–492, <https://doi.org/10.1137/0113030>, 1965.

766 Kurtz, T., Eberhard, P., Henninger, C., and Schiehlen, W.: From Neweul to Neweul-M2: symbolical equations of motion for multibody system
767 analysis and synthesis, *Multibody System Dynamics*, 24, 25–41, <https://doi.org/10.1007/s11044-010-9187-x>, 2010.

768 Kurtz, T. and Eberhard, P.: Symbolic Modeling and Analysis of Elastic Multibody Systems, in: *International Symposium on Coupled Methods*
769 in Numerical Dynamics Split, Croatia, September 16-19, 2009.

770 Lange, C., Kövecses, J., and Gonthier, Y.: Benchmarking of Multibody System Simulations: Points to Consider, in: *CcToMM Symposium*
771 on Mechanisms, Machines, and Mechatronics, Saint-Hubert, Québec, 2007.

772 Lemmer, F.: Low-order modeling, controller design and optimization of floating offshore wind turbines., Ph.D. thesis, Universit at Stuttgart,
773 <http://elib.uni-stuttgart.de/handle/11682/10543>, 2018.

774 MBDyn: <https://www.mbdyn.org/>, accessed: 2022-03-19, 2022.

775 Merz, K. O.: STAS Aeroelastic 1.0 - Theory Manual., Tech. rep., Trondheim, SINTEF Energi AS., 2018.

776 MotionGenesis: MotionGenesis™ Kane Tutorial, Tech. rep., Motion Genesis LLC, www.motiongenesis.com, 2016.

777 Øye, S.: Fix Dynamisk, aeroelastisk beregning af vindmøllevinger, Report AFM83-08, Fluid Mechanics, DTU, 1983.

778 Pöschke, F., Gauterin, E., Kühn, M., Fortmann, J., and Schulte, H.: Load mitigation and power tracking capability for wind turbines using
779 linear matrix inequality-based control design, *Wind Energy*, 23, 1792–1809, <https://doi.org/10.1002/we.2516>, 2020.

780 Reckdahl, K. and Mitiguy, P.: Autolev Tutorial, Tech. rep., OnLine Dynamics Inc., Sunnyvale CA, 1996.

781 Schwertassek, R. and Wallrapp, O.: *Dynamik flexibler Mehrkörpersysteme*. [in German], Friedr. Vieweg & Sohn, Braunschweig, 1999.

782 Shabana, A.: *Dynamics of Multibody Systems*, *Dynamics of Multibody Systems*, Cambridge University Press, 2013.

783 Simani, S.: Advanced Issues of Wind Turbine Modelling and Control, *Journal of Physics - Conference series*, 659, 2015.

784 Simo, J.: A finite strain beam formulation. The three-dimensional dynamic problem. Part I, *Computer Methods in Applied Mechanics and*
785 *Engineering*, 49, 55–70, [https://doi.org/10.1016/0045-7825\(85\)90050-7](https://doi.org/10.1016/0045-7825(85)90050-7), 1985.

786 SIMPACK: <https://www.3ds.com/products-services/simulia/products/simpack/>, accessed: 2022-03-19, 2022.

787 Sønderby, I. and Hansen, M. H.: Open-loop frequency response analysis of a wind turbine using a high-order linear aeroelastic model, *Wind*
788 *Energy*, 17, 1147–1167, <https://doi.org/10.1002/we.1624>, 2014.

789 SymPy: <https://www.sympy.org/>, 2021.

790 Verlinden, O., Kouroussis, G., and Conti, C.: EasyDyn: a framework based on free symbolic and numerical tools for teaching multibody
791 systems, in: *Multibody Dynamics 2005, ECCOMAS Thematic Conference*, 2005.

792 Wallrapp, O.: Standard Input Data of Flexible Members in Multibody Systems, in: *Advanced Multibody System Dynamics. Solid Mechanics*
793 *and Its Applications*, edited by Schiehlen, W., vol. 20, pp. 445–450, Springer, Dordrecht, https://doi.org/10.1007/978-94-017-0625-4_33,
794 1993.

795 Wallrapp, O.: Standardization of flexible body modeling in multibody system codes, part i: Definition of standard input data., *Journal of*
796 *Structural Mechanics*, 22, 283–304, 1994.

797 Wallrapp, O. and Schwertassek, R.: Representation of geometric stiffening in multibody system simulation, *International Journal for Numerical*
798 *Methods in Engineering*, 32, 1833–1850, <https://doi.org/10.1002/nme.1620320818>, [10.1002/\(ISSN\)1097-0207](https://doi.org/10.1002/(ISSN)1097-0207), 1991.